

A small, computationally flexible network produces the phenotypic diversity of song recognition in crickets

Jan Clemens^{1,*}, Stefan Schöneich^{2,5}, Konstantinos Kostarakos^{3,5}, R. Matthias Hennig⁴, Berthold Hedwig⁵

Affiliations:

1. European Neuroscience Institute Göttingen – A Joint Initiative of the University Medical Center Göttingen and the Max-Planck Society, Grisebachstrasse 5, Göttingen, 37077, Germany (clemensjan@gmail.com)
2. Friedrich-Schiller-University Jena, Institute for Zoology and Evolutionary Research, Erbertstrasse 1, 07743 Jena, Germany (stefan.schoeneich@uni-jena.de)
3. Institute of Biology, University of Graz, Universitätsplatz 2, 8010-Graz, Austria (konstantinos.kostarakos@uni-graz.at)
4. Humboldt-Universität zu Berlin, Department of Biology, Philippstr. 13, 10115 Berlin, Germany (matthias.hennig@rz.hu-berlin.de)
5. University of Cambridge, Department of Zoology, Downing Street, CB2 3EJ Cambridge, United Kingdom (bh202@cam.ac.uk)

* correspondence: clemensjan@gmail.com

Acknowledgments:

We thank Biswa Sengupta for discussions during an early phase of the project.

Funding:

BH: Biotechnology and Biological Science Research Council (grant: BB/J01835X/1)

KK: Royal Society (Newton International Fellowship); BBSRC

MH: DFG: HE 2812/4-1 & HE 2812/5-1 (SPP2205), Leibniz Association: SAW 2012-MfN-3 (Genart)

JC: DFG CL 596/1-1 (32951824), SPP 2205 (430158535)

Abstract

How neural networks evolve to recognize species-specific communication signals is unknown. One hypothesis is that novel recognition phenotypes are produced by parameter variation in a computationally flexible “mother network”. We test this hypothesis in crickets, where males produce and females recognize mating songs with a species-specific pulse pattern. Whether the song recognition network in crickets is computationally flexible to recognize the diversity of pulse patterns and what network properties support and constrain this flexibility is unknown. Using electrophysiological recordings from the cricket *Gryllus bimaculatus*, we built a model of the song recognition network that reproduces the network dynamics as well as the neuronal and behavioral tuning for that species. An analysis of the model’s parameter space reveals that the network can produce all recognition phenotypes known in crickets and even other insects. Biases in phenotypic diversity produced by the model are consistent with the existing behavioral diversity in crickets, and arise from computations that likely evolved to increase energy efficiency and robustness of song recognition. The model’s parameter to phenotype mapping is degenerate – different network parameters can create similar changes in the phenotype – which is thought to support evolutionary plasticity. Our study suggest that a computationally flexible mother network could underlie the diversity of song recognition phenotypes in crickets and we reveal network properties that constrain and support behavioral diversity.

Introduction

Behavior is driven by the recognition and evaluation of sensory stimuli. For instance, hunting requires the detection and tracking of prey; communication requires the recognition of the sounds, pheromones or visual displays that serve as signals. The diversity of animal behaviors across taxa betrays the capacity of sensory systems to evolve and adapt to reliably and specifically recognize a wide variety of signal patterns. Genes that control evolutionarily divergent behaviors within a species group have been identified (Blankers et al., 2018; Ding et al., 2016; Xu and Shaw, 2019) and progress has been made in linking these genetic changes to the neuronal mechanisms underlying pattern recognition. Circuit evolution is well understood when behaviors are driven by signals recognized through the response specificity of primary afferent neurons: For instance, by altering the structure of olfactory receptor proteins (Prieto-Godino et al., 2017; Ramdya and Benton, 2010) or by changing the synaptic weights of a labelled line input to a pre-motor neuron (Auer et al., 2020; Prieto-Godino et al., 2017; Seeholzer et al., 2018) a different odorant will trigger a specific behavioral response. Equivalently, simple behavioral preferences for visual or acoustic stimuli can be set by the wavelength or frequency tuning of visual or auditory receptor neurons (Kocher, 2004; Kostarakos et al., 2008; Riabinina et al., 2011; Wytenbach et al., 1996).

However, many behaviors are driven by complex temporal and spatial stimulus patterns, whose recognition is based on the comparison of neural activity across time and space. For these behaviors, linking genetic changes to the underlying neural computation is challenging since it requires a mapping from circuit parameters to recognition phenotype. One prominent behavior involving the recognition of complex temporal patterns is acoustic communication. Many animals – monkeys, mice, bats, birds, frogs, crickets, grasshoppers, katydids, fruit flies – produce species-specific songs to attract and woo conspecifics of the other sex (Baker et al., 2019; Bradbury and Vehrencamp, 2011; Kostarakos and Hedwig, 2014; Neunuebel et al., 2015). The structure of song as well as the behavioral preference for it can evolve rapidly during speciation events (Blankers et al., 2015; Mendelson and Shaw, 2005), giving rise to the large diversity of species-specific songs. While genes linked to song pattern generation have been identified (Ding et al., 2016; 2019; Turner et al., 2013; Xu and Shaw, 2019), it is unclear how song pattern recognition adapts to drive speciation. During the evolution of acoustic communication, song recognition networks must be selective and modifiable to adapt to changing signal patterns (Wagner, 2008). The ability of artificial neural networks to generate different recognition phenotypes has been investigated using abstract modelling approaches in invertebrates and vertebrates (Clemens and Hennig, 2013; Hennig et al., 2014; Ryan et al., 2001). However, it is crucial to extend these analyses to specific biological networks (Destexhe and Marder, 2004; Gutierrez et al., 2013), since implementation details determine the range of phenotypes an abstract algorithm can produce.

We here examine the computational capacity of a song recognition network in crickets. The diverse song preferences have been extensively mapped in multiple species (e.g. (Bailey et al., 2017; Cros and Hedwig, 2014; Gray et al., 2016; Hennig, 2003; 2009; Hennig et al., 2016; Rothbart and Hennig, 2012a; 2012b)) and the song recognition network for one particular species is known (Kostarakos and Hedwig, 2012; Schöneich et al., 2015). The computation performed by this system – the evaluation of a repetitive pulse pattern – is a

common denominator of many communication systems from insects to fish and frogs (Baker et al., 2019; Carlson and Gallant, 2013; Gerhardt and Huber, 2002). Moreover, circuits analyzing temporal patterns of amplitude modulations are likely building blocks for recognizing the more complex acoustic communication signals found in vertebrates like songbirds or mammals (Aubie et al., 2012; Coffey et al., 2019; Comins and Gentner, 2014; Gentner, 2008; Neunuebel et al., 2015). Insights from crickets are therefore relevant for studies of the evolution of communication systems in general.

Cricket song consists of a sinusoidal carrier frequency, modulated in amplitude with temporal structure on short ($<100\text{ms}$) and long ($>100\text{ms}$) timescales (Fig. 1A). On the short timescale, the song consists of trains of sound pulses with a species-specific pulse duration and pulse pause. On the long timescale, pulse trains are either continuous (trills) or interrupted at regular intervals by a longer chirp pause. The pulse pattern on the short timescale – and the female preference for it – is compactly described in a two-dimensional parameter space spanned by pulse duration and pause (Fig. 1B, C). Analysis of the female preference of more than 20 cricket species revealed three principal types of preference, defined by selectivity for specific features of the pulse pattern (Fig. 1B): pulse duration, pulse period (duration plus pause), and pulse duty cycle (duration divided by period, corresponds to signal energy) (Hennig et al., 2014). A fourth type of selectivity – for pulse pause – has not been reported in crickets and is only known from katydids (Schul, 1998).

The neuronal circuit that computes the behavioral preference for the pulse pattern has been revealed in the cricket *Gryllus bimaculatus* (Kostarakos and Hedwig, 2012; Schöneich et al., 2015). In this species, the selectivity for a narrow range of pulse periods is created in a network of 5 neurons and 6 synaptic connections by combining a delay-line with a coincidence-detector (Fig. 1D). The ascending auditory neuron 1 (AN1) is tuned to the carrier frequency of the male calling song and provides the input to a small, four-cell network in the cricket brain. Driven by AN1, the local neuron 2 (LN2) inhibits the non-spiking neuron LN5, which functions as delay-line and produces a post-inhibitory rebound driven by the end of each sound pulse. The coincidence-detector neuron LN3 receives direct excitatory input from AN1 and a delayed excitatory input driven by the rebound of LN5; it fires strongly only if both inputs coincide. Lastly, the feature detector neuron LN4 integrates excitatory input from LN3 and inhibitory input from LN2, which sharpens its selectivity. LN4's selectivity for pulse patterns matches the phonotactic behavior of females (Fig. 1E).

We here asked whether the implementation of the song recognition mechanism in *G. bimaculatus* (Fig. 1 D) has the capacity to produce the full diversity of recognition phenotypes known from crickets and other insects (Fig. 1B), and what specific circuit properties support and constrain this capacity. Based on electrophysiological recordings (Kostarakos and Hedwig, 2012; Schöneich et al., 2015) we fitted a computational model that reproduces the response dynamics and the tuning of the neurons in the song recognition network. By exploring the network properties over a wide range of parameters, we show that the network of *G. bimaculatus* can be modified to produce all types of preference functions known from crickets (and other insect species). The phenotypic diversity produced by the network is consistent with the diversity of recognition phenotypes in crickets and is shaped by computations that reduce responses – adaptation or inhibition.

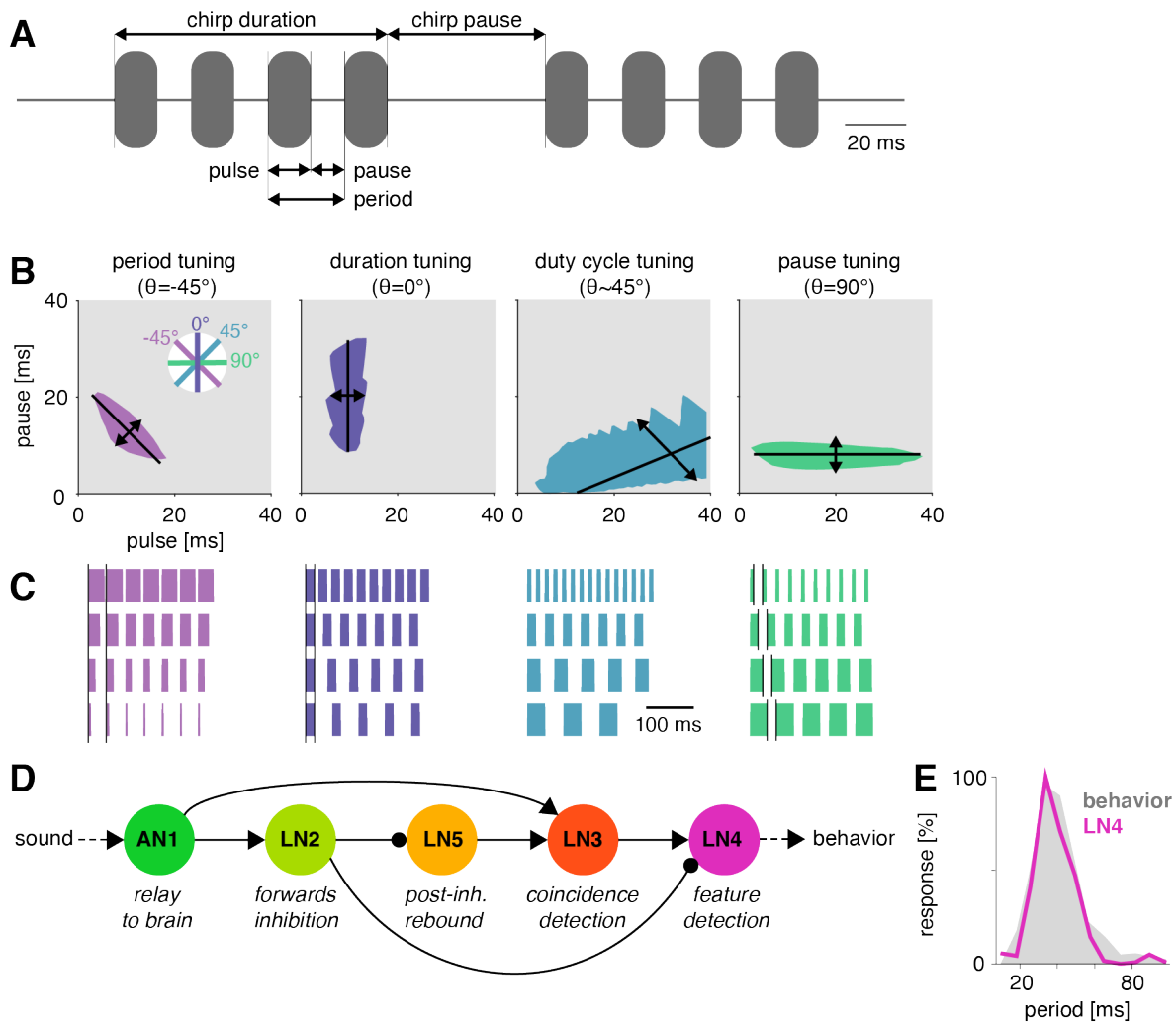


Figure 1: Song structure and song preference in crickets, and the song recognition network of *Gryllus bimaculatus*.

A Parameters of the temporal pattern of cricket song. Short sound pulses are interleaved by pulse pauses. The pulse period is given by the sum of pulse duration and pulse pause. The pulse duty cycle corresponds to signal energy and is given by the ratio between pulse duration and period. In many species, pulses are grouped in chirps and interleaved by a chirp pause, while other species produce continuous pulse trains, called trills.

B The behavioral tuning for pulse patterns can be characterized using response fields, which mark the set of behaviorally preferred pulse parameters in a two-dimensional diagram spanned by pulse duration and pause duration. Four principal response types are defined based on tolerance (black lines) and selectivity (double headed arrows) for stimulus parameters, leading to specific orientations of the response field (see left inset): For instance, period tuning (purple) is defined by selectivity for pulse period and tolerance for pulse duty cycle, giving an orientation of the response field of -45° . Duration tuning (lilac), duty cycle (cyan), and pause tuning (green) are defined correspondingly (from (Clemens and Hennig, 2013; Hennig et al., 2014)).

C Example stimulus series illustrating the stimulus features each response type in B is selective for. Vertical black lines mark the pulse train feature that is constant for each row. For duty cycle (cyan), the ratio between pulse duration and period is constant.

D Song recognition network in the brain of *G. bimaculatus*. The network consists of 5 neurons, each with a specific computational role, which are connected in a feed-forward manner using excitation (pointed arrowheads) and inhibition (round arrowheads). The excitatory ascending neuron 1 (AN1) relays information from auditory receptors in the prothorax to the brain. The inhibitory local neuron 2 (LN2) inverts the sign of AN1 responses. LN2 inhibits the non-spiking LN5 neuron, which produces a post-inhibitory rebound. LN3 acts as a coincidence detector for excitatory input from AN1 and LN5. Input delays are tuned such that LN3 is maximally driven by the conspecific pulse train with a pulse period of 30-40ms. LN4 integrates excitatory input from LN3 and inhibitory input from LN2 to further sharpen the output of the network.

E Tuning for pulse period in LN4 (purple) matches the phonotaxis behavior (gray) of *G. bimaculatus* females (D, E adapted from (Schöneich et al., 2015)).

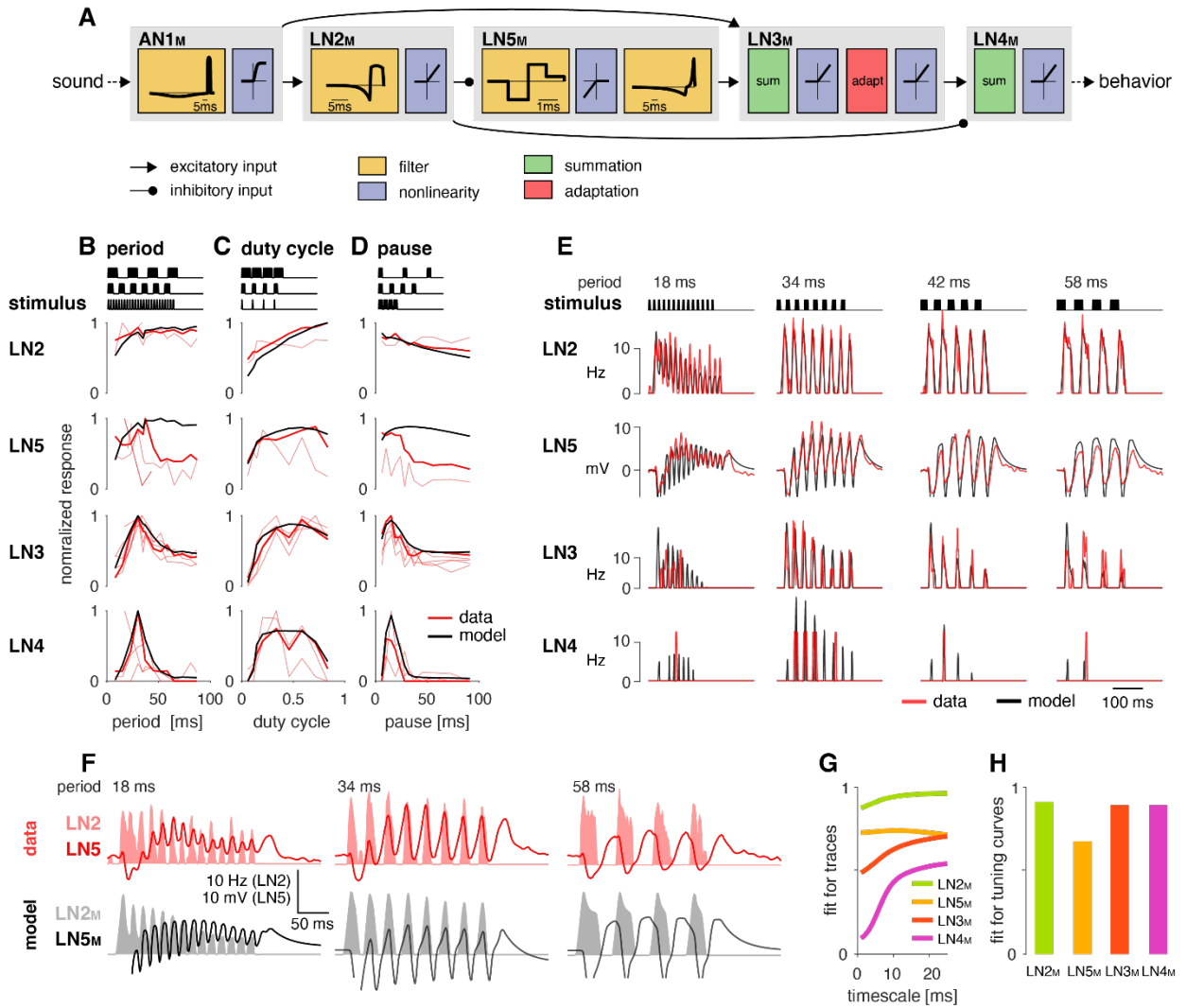
Results

A computational model of the song recognition network in *G. bimaculatus*.

We tested whether the delay-line and coincidence-detector network of the cricket *G. bimaculatus* (Fig. 1D) can be modified to produce the known diversity of preference functions for cricket calling songs (Fig. B). We fitted a computational model based on intracellularly recorded responses of the network's neurons for pulse trains, but we did not aim for a biophysical implementation of the neurons, since their ion channels and conductances are not known. Instead, we reproduced the responses of individual neurons using a phenomenological modelling approach using four elementary computations (Fig. 2A): 1. linear filtering, 2. sigmoidal or rectifying nonlinearities, 3. adaptation, and 4. linear transmission with a delay. The computational steps – for instance, whether a neuron had an integrating or a differentiating filter (Fig. S1) – were selected such that each neuron's response dynamics could be reproduced (Fig. 2A, S2, Table 1). The model parameters were then numerically optimized to fit each neuron's response dynamics and tuning (Fig. 2B-H). Neurophysiological data used for fitting were the time-varying firing rate for the spiking neurons LN2, LN3, and LN4, and the membrane voltage for the non-spiking LN5 neuron, all in response to periodical pulse trains with different pulse durations and pauses (Kostarakos and Hedwig, 2012; Schöneich et al., 2015). A detailed description of the model parameters, of the data used for fitting, and of the fitting procedure are given in Methods, Fig. S1, S2, and Table 1.

The model faithfully reproduces the neural responses.

The fitted model closely reproduced the responses of the network neurons to stimuli from the electrophysiological data set (Fig. 2B-H). To quantify model performance, we assessed the match in the dynamics and in the tuning between the neuronal and the model responses. First, we computed the squared correlation coefficient (r^2) between the recorded and the modelled responses at different timescales (Fig. 2G). At short timescales, the measure is sensitive to precise response timing whereas at longer timescales it reflects the match in the response magnitude. R^2 is high across all timescales for the model neurons (indexed with "M") LN2_M, LN3_M, and LN5_M, which respond in the biological network with multiple spikes or sustained membrane voltage deflections to a pulse. By contrast, LN4 produces only few and irregularly timed spikes during a pulse, and therefore r^2 is highest for timescales exceeding the duration of a typical pulse (15 ms). Second, we calculated the match between the tuning curves derived from the data and the model (Fig. 2H). The model excellently reproduced the tuning curves of LN2_M, LN3_M and LN4_M. Performance is somewhat lower for LN5_M since the model produced overly strong rebound responses for patterns with long pulse periods and pauses (Fig. 2B, D). In the data, the rebound amplitude is also highly variable across individuals even though the tuning of responses downstream of LN5 – in LN3 and LN4 – is not (Fig. 2B-D). This indicates that the network is robust to small changes in rebound amplitude and that it primarily relies on rebound timing, which is well reproduced in our model (Fig. 2E-G). This is confirmed by the excellent reproduction of the response dynamics and tuning for the downstream neurons LN3_M and LN4_M.



To further assess the model's performance, we examined each model neuron's responses over a wide range of pulse and pause durations that covered the range of song parameters found in most cricket species (Weissman and Gray, 2019). There exist no electrophysiological data for such a wide range of stimuli but the behavioral data from *G. bimaculatus* indicate that the neural responses should change smoothly with the song parameters (Grobe et al., 2012; Hennig et al., 2014; Kostarakos and Hedwig, 2012). The responses of all neurons in the model – presented as two-dimensional response fields which depict the response rate for each duration-pause combination in the set of test stimuli – are consistent with this expectation (Fig. 3A). Discontinuities in the responses with a stimulus parameter stem from the discrete nature of the stimulus, because the number of pulses per train changes with pulse duration and pause (Fig. S3A, B). The response fields illustrate the gradual transformation of tuning in the network: LN2_M at the beginning of the network responds best to stimuli with large duty cycles, i.e., stimuli with long pulse durations and short pauses. Following the network from LN5_M over LN3_M to LN4_M, the responses to large duty-cycle stimuli attenuate and the pulse period tuning becomes more and more prominent, with LN4_M ultimately being selective for a narrow range of pulse periods.

In summary, our model reproduces the characteristic response features of each neuron in the biological network. Using this model of the song recognition mechanism in *G. bimaculatus* we can now test whether the network has the capacity to produce the behavioral preferences of other cricket species and identify the parameters that determine the network's preference.

The network can be tuned to produce all known song preferences of crickets.

To determine the diversity of behavioral preferences the network can produce, we examined the response fields of different model variants obtained by altering all model parameters – for instance, the weight and delay of inputs or the amplitude or duration of filters. Each model variant was generated by randomly picking values for each of 41 parameters from an interval around the parameter values of the fit to *G. bimaculatus* (see Methods for details and Table 1 in Methods). Biophysical parameters of a neuron type can vary tenfold even within a species (Goaillard et al., 2009; Schulz et al., 2007) and we therefore chose an interval of 1/10 to 10 times the values from *G. bimaculatus*. Initial experiments with a wider range (1/100 to 100 fold) yielded qualitatively similar results but a large fraction of untuned or unresponsive models. Delay parameters were randomly picked from an interval between 1 and 21 ms. Delay parameters correspond to the delay added to a neuron's inputs (Fig. S1F) and were optimized during fitting to match the timing of the responses of the neuron's outputs. They therefore account not only for axonal transduction and synaptic transmission delays but also for delays arising from low-pass filtering or integration of inputs to the spiking threshold (Creutzig et al., 2010; Zhou et al., 2019), justifying the extending range of values. The preference properties of the network models with randomized parameter sets were characterized using response fields, which are given as the response rate of the network's output neuron LN4_M to pulse trains with all combinations of pulse durations and pauses between 1 and 80 ms (Fig. 4A). We generated 1.58 million model variants, 90% of these were responsive and selective and used for all further analyses.

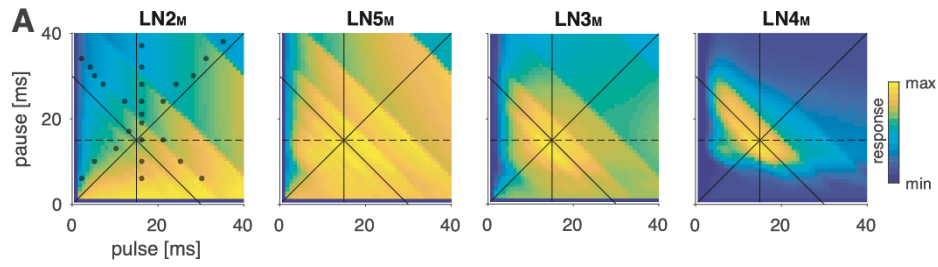


Figure 3: Model responses to novel pulse train stimuli.

Responses of the model neurons for stimuli with different combinations of pulse and pause durations (1-40 ms, 1600 stimuli per response field, color code corresponds to response magnitude). Each response field depicts the firing rate (for LN2M-4M) or the voltage of the rebound (for LN5M) of model neurons. Pulse trains had a fixed duration of 140 ms and were interleaved by a pause of 200 ms, mimicking the chirp structure of *G. bimaculatus* calling song. Anti-diagonal step-like patterns in the response fields arise from changes in the number of pulses per train (Fig. S3A, B). Although the data set used for fitting did not include stimuli with long pulse durations, the model predicts the weak response known from the behavior for these stimuli (horizontal dashed line). Solid black lines indicate stimuli with 15 ms pulse duration (vertical), 30 ms pulse period (anti-diagonal), or 0.5 pulse duty cycle (diagonal). Dots in the leftmost panel mark the stimuli used for fitting.

As a first step towards characterizing the types of tuning the network can produce, we assessed the preferred pulse duration and pause of each of the ~1.4 million selective model variants (Fig. 4A). We find that preferences cover the full range of pulse and pause combinations tested (Fig. 4B). However, the model variants do not cover the preference space uniformly but are biased to prefer patterns with short pulse durations, short periods, and low duty cycles (<0.5) (Fig. 4C). Thus, the network can flexibly produce a wide variety of recognition phenotypes, but intrinsic constraints bias the preferences towards specific stimulus patterns.

The preferred pulse duration and pause only incompletely describe a network's recognition phenotype. Behavioral analyses in crickets and other insects (Deutsch et al., 2019; Hennig et al., 2014; Schul, 1998) have identified four principal types of tuning (Fig. 1B), which are defined by the orientation of the response field in the two-dimensional parameter space spanned by pulse duration and pause (Fig. 4A). Typically, response fields are well approximated by ellipses, with the elongated major axis defining stimulus parameters the network is most tolerant for, and the shorter minor axis defining parameters the network is most selective for. Specifically, *duration tuning* is defined as selectivity for pulse duration and tolerance for pause (Fig. 1C, lilac). This corresponds to the response field's major axis being parallel to the pause axis (defined as an orientation θ of 0° , see inset in Fig. 4D). By contrast, *pause tuning* (Fig. 1C, green) corresponds to an orientation θ of 90° , with the response field's major axis extending parallel to the pulse duration axis. Pulse period and duty cycle tuning correspond to response fields with diagonal and anti-diagonal orientations, respectively. *Period tuning* (Fig. 1C, purple) is given by an anti-diagonal orientation ($\theta = -45^\circ$), indicating selectivity for pulse period and tolerance for duty cycle. Last, *duty-cycle tuning* (Fig. 1C, cyan) is given by diagonal alignment ($\theta = 45^\circ$) and selectivity for duty cycle but tolerance for period. Models were classified as belonging to any of the four principal types based on two criteria: The orientation of the major (tolerant) axis of their response fields had to be within $\pm 5^\circ$ of that of the principal types (Fig. 4D) and they had to be narrowly tuned along the minor axis (see Methods for details). Note that our results do not depend critically on the specific choice of inclusion criteria. For instance, removing the narrowness criterion produced qualitatively similar results.

When examining the orientation and selectivity for each response field, we find that the network can produce response fields with any orientation in the stimulus space – including the orientations corresponding to the four principal types (Fig. 4D). However, the different preference types did not occur with the same frequency: Most network variants produced pulse duration tuning (84%), period and duty cycle tuning were less frequent (9 and 5%, respectively), and pause tuning was rare (2%). Response profiles from each principal type cover the full range of preferred durations and pauses indicating that specific types of tuning can be created everywhere in the tested parameter space (Fig. 4E). The rarity of pause tuning is consistent with the bias to prefer short pulse durations observed above (Fig. 4C), since pause tuning requires response fields that extend parallel to the duration axis.

Our analysis of different model variants based on a delay-line and coincidence-detector, defined by the same set of elementary computations in each model neuron but different sets of parameters, reveals that this song recognition network can produce all known preference

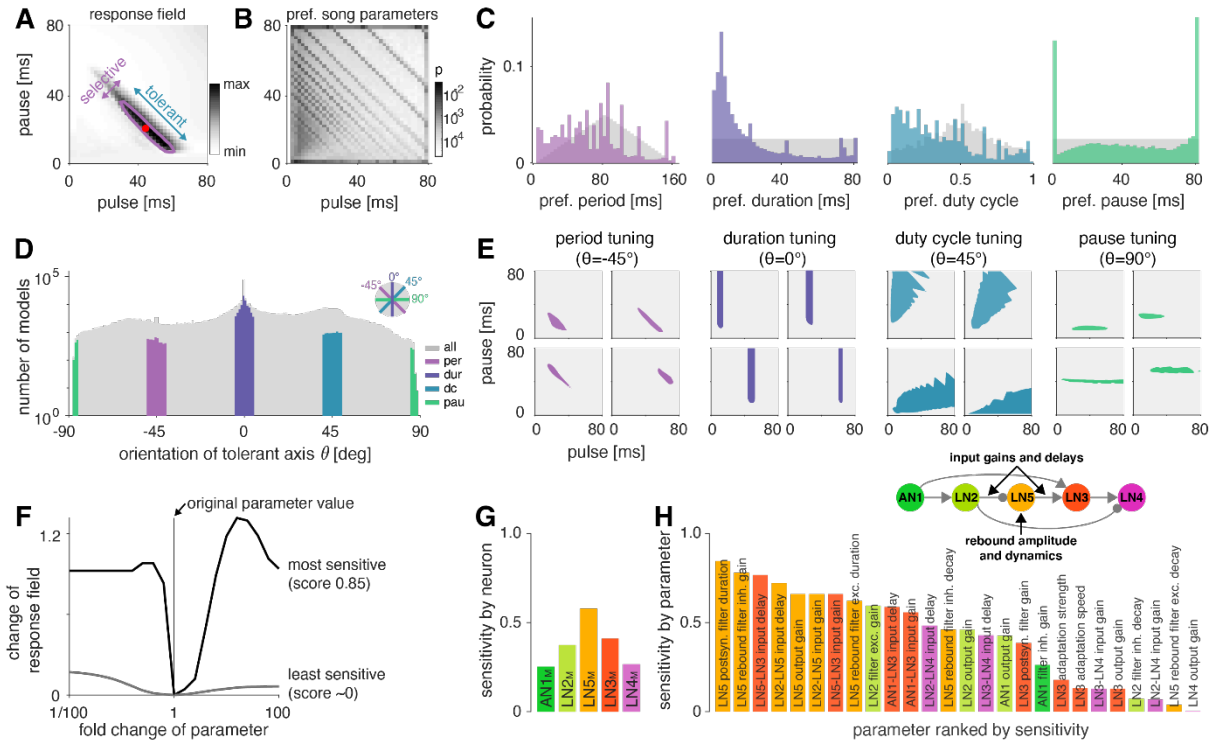


Figure 4: The network generates the diversity of response profiles known from crickets and other insects.

A Response field generated from a model variant with randomized parameters. Response magnitude coded in color (see color bar). Tuning was characterized in terms of the preferred pulse and pause durations (red dot) and as tolerant (blue) or selective (purple) directions in the stimulus field. This example is period tuned (purple contour marks the 75% response level) and the set of preferred stimuli is oriented at -45° (see inset in D for a definition of the angles), corresponding to selectivity for period (purple) and tolerance for duty cycle (cyan).

B Distribution of preferred pulse and pause parameters for all model variants generated from randomized parameter combinations (color coded, see color bar). Anti-diagonal patterns arise from the discrete nature of pulse trains (Fig. S3A, B). Models that prefer pauses of 0 ms correspond to models that prefer constant tones. Enrichment of models that prefer the maximally tested pause of 80 ms indicates that the network can generate preference for longer pauses than we had tested. Preferences cover the stimulus field.

C Distribution of preferred pulse parameters (left to right: pulse period, duration, duty cycle and pause). Grey histograms correspond to the distributions expected from uniform sampling of stimulus space – deviations from this distribution indicate response biases. The network is biased to produce preferences for short pulse periods and durations, low duty cycles, and long pauses. The peaks in the histograms arise from the discrete nature of pulse trains (Fig. S3A, B) or from boundary effects (see B).

D Distribution of the orientation of the response fields (see A) for all model variants (log scale). The grey histogram shows the distribution for all models. Colored bars show to the subset of models that correspond to the four principal response types (1B) based on our criteria (see Methods). The network can produce response fields at all angles, including the four principal types of tuning for period, duration, duty cycle, and pause. Response fields with small angles around 0° , corresponding duration tuning, occur most often.

E Examples of tuning profiles for pulse period, duration, duty cycle, and pause. Profiles for all tuning types cover the examined stimulus space.

F To identify model parameters useful for controlling network tuning, we modified each individual model parameter between 1/100 and 100-fold and calculated the change in the response field. The sensitivity score quantifies how much changing a parameter's value changes the response field. Examples shown are the parameters with the highest (LN5_M postsynaptic filter duration, black) and lowest non-zero sensitivity (LN5_M rebound filter excitatory decay, grey) (see H).

G Average sensitivity scores by neuron. LN5_M has the highest score, it most strongly shapes network tuning, consistent with the rebound and coincidence detection being the core computational motif of the network.

H Model parameters ranked by sensitivity score. Parameters that induce no or only a single step-like change in the response field were excluded. Color indicates cell type (same as in G). Parameters of LN5_M (bright orange) and LN3_M (dark orange) rank highest, demonstrating the importance of the rebound and coincidence detection for shaping model tuning. The model schematic (inset) highlights the most important types of parameters.

types over the range of stimulus parameters relevant for crickets. This phenotypic flexibility suggests that the network may form the basis for the diversity of song recognition phenotypes. We therefore sought to identify model parameters that support that diversity, i.e., parameters that change the preference for pulse period or that switch the preference from one type to another. We also looked for parameters that constrain the diversity, e.g. parameters that induce a bias towards low duty cycles (Fig. 4B-D).

Post-inhibitory rebound properties and coincidence timing are key parameters that shape preferences.

To determine key parameters that control the network tuning and to identify the computational steps that induce the preference bias, we systematically examined the effect of changing individual model parameters on the response fields. We swept each parameter individually in 21 log-spaced steps over an interval of 1/100 to 100 fold around the values from the original fit (Fig. 4F). We then calculated a sensitivity score for each parameter as the average change in the response field of the network's output neuron, LN4_M, over the parameter sweep (see Methods). Parameters that when changed produced mostly unselective or unresponsive models were excluded from subsequent analyses as were parameters that only induced one or two sudden changes in the response fields. For instance, parameters that control the firing threshold of AN1 were excluded because they turn the input to the network on or off – this produces a large, step-like change in the response field and many unresponsive models. Our sensitivity analysis thereby focuses on parameters suitable for controlling the network's tuning, i.e., whose change induces smooth shifts in the model responses while retaining responsiveness and selectivity.

The topology of the pattern recognition network is defined by five neurons (Fig. 1D). As a first step, we sought to evaluate the importance of each neuron for controlling the network tuning, by averaging the sensitivity scores for the parameters of each neuron (Fig. 4G). This revealed that all five neurons affected tuning and that the network responses were most sensitive to parameters of the non-spiking neuron LN5_M, which generates the delayed post-inhibitory rebound. The importance of LN5_M is consistent with the idea that the rebound and coincidence detection form the core computations of the network (Schöneich et al., 2015), since the dynamics of the rebound response directly influence what stimulus features result in simultaneous inputs to the coincidence detector neuron LN3_M.

To identify important parameters for tuning the network we ranked them by their sensitivity score (Fig. 4H). In line with the above analysis for each neuron, ten of the eleven top-ranked parameters directly affect the inputs to LN3_M. Among these are the delays and gains for the connections upstream of LN3_M (AN1_M→LN3_M, LN2_M→LN5_M, LN5_M→LN3_M), since they affect the timing and the amplitude of inputs to LN3_M. Another group of important parameters affects the dynamics and amplitude of the rebound response in LN5_M: First, the duration of the “postsynaptic” filter of LN5_M (Fig. S2), which is required to reproduce the adapting and saturating dynamics of the inputs to LN5_M, visible as negative voltage components in recordings of LN5_M (Schöneich et al., 2015). Second, the gain of the inhibitory and the duration of the excitatory lobe of the rebound filter that produces the post-inhibitory rebound (Fig. S1E, S2). A modified sensitivity analysis, in which we changed combinations of two

parameters at a time produced a similar parameter ranking, confirming the robustness of these results (Fig. S3C).

Our sensitivity analysis revealed key parameters that change the tuning of the network, but did not address their specific effect, for instance on the preference for specific pulse durations or periods (Fig. 4E). This is however crucial for understanding which network parameters need to be modified to produce a specific phenotype, and where the bias for stimuli with low duty cycles (short pulses and long pauses) arises (Fig. 4B-D). We therefore examined the specific effects of some of the top-ranked parameters (Fig. 4H) on the tuning of the network.

Relative timing of inputs to the coincidence detector controls pulse period preference.

Four of the seven most important parameters affect the timing of inputs to the coincidence detector neuron LN3. Three of these parameters are the delays of the $AN1_M \rightarrow LN3_M$, the $LN2_M \rightarrow LN5_M$, and the $LN5_M \rightarrow LN3_M$ connections. The fourth parameter – the duration of the filter that shapes input adaptation in $LN5_M$ – also affects the input delays to $LN3_M$ (Fig. S4). The delay between the spikes from $AN1_M$ and the rebound from $LN5_M$ in $LN3_M$ strongly affects network tuning since it determines which pulse train parameters produce coincident inputs required for driving spikes in $LN3_M$ (Fig. 5A). Increasing this delay – for instance by delaying the rebound from $LN5_M$ – increases the preferred pulse periods in $LN3_M$ (Fig. 5B). This delay was hypothesized to be the core parameter that tunes *G. bimaculatus* to a pulse period of 30-40 ms (Schöneich et al., 2015) and our sensitivity analysis identifies this parameter as crucial for shaping the network's tuning.

Interestingly, changing the rebound delay has differential effects in $LN3_M$ and in the output neuron of the network, $LN4_M$. In $LN3_M$, increasing the rebound delay changes both duration and pause preference and increases the preferred pulse period without changing the duty cycle preference (Fig. 5C, D). However, in $LN4_M$, a longer rebound delay only affects pause preference, but not duration preference and thereby reduces the preferred duty cycle from 0.5 to 0.25 (Fig. 5D, S3D). This reduction of the preferred duty cycle is a correlate of the low duty cycle bias observed in the network (Fig. 4C). We therefore investigated the origin of this effect more closely.

$LN4_M$ receives excitatory input from $LN3_M$ and inhibitory input from $LN2_M$, and applies a threshold to the summed inputs (see Fig. 2A, S2). To determine which computation in $LN4_M$ reduces the preferred duty cycle, we removed the inhibition from $LN2_M$ and the threshold in $LN4_M$'s output nonlinearity. While the threshold has only minor effects on tuning, removing the inhibition is sufficient to restore the preference for intermediate duty cycles in $LN4_M$ (Fig. 5B-D, blue). This implies that the inhibition from $LN2_M$ suppresses the responses to high duty cycles in $LN4_M$. We find that changes in the strength and in the timing of excitatory inputs from $LN3_M$ to $LN4_M$ with duty cycle contribute to this suppression (Fig. 5E, F). First, the excitatory inputs from $LN3_M$ weaken with increasing duty cycle, leading to a relatively stronger impact of the inhibition from $LN2_M$ on the responses of $LN4_M$ (Fig. 5F). Second, the excitatory inputs from $LN3_M$ arrive later with increasing duty cycle, resulting in a more complete overlap with the inhibition from $LN2_M$ and therefore to a more effective suppression of $LN4_M$ spiking responses (Fig. 5E, F).

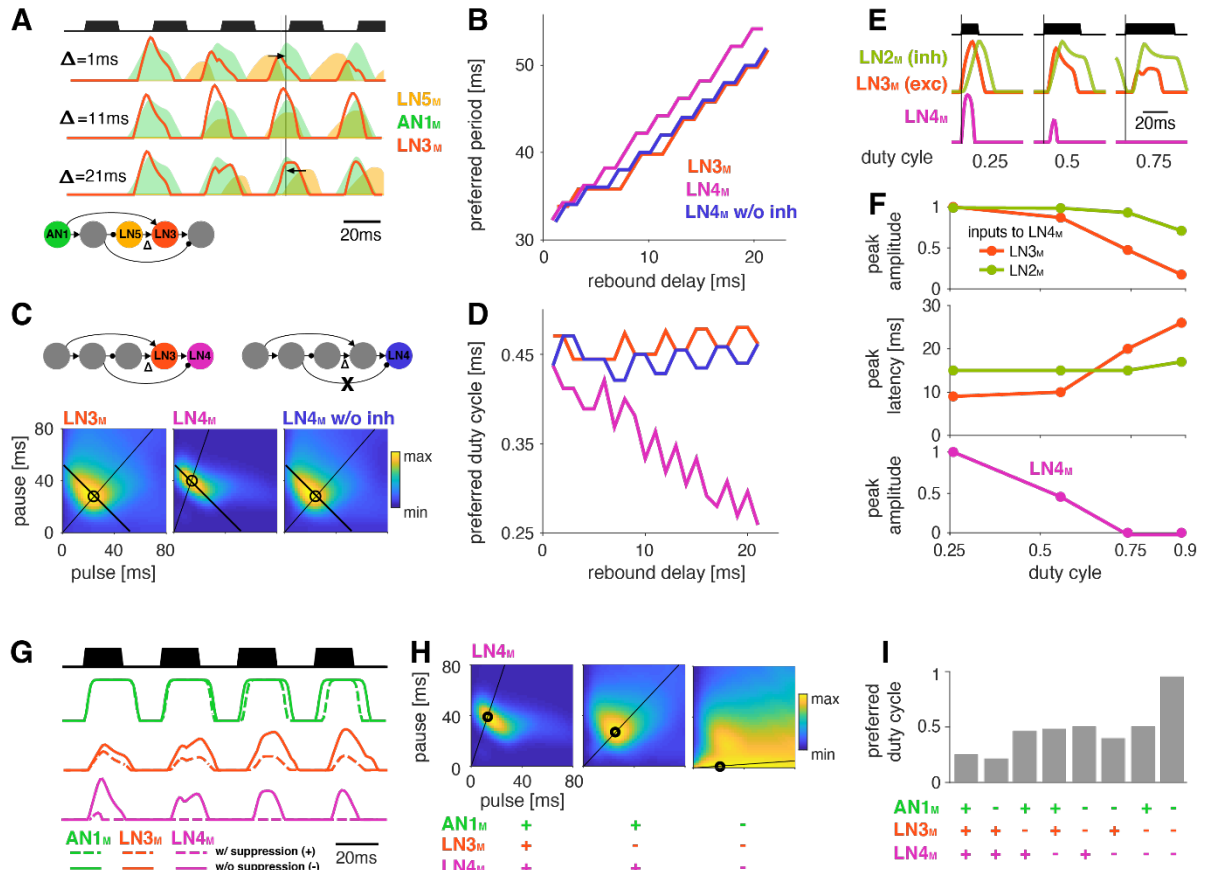


Figure 5: Input delays and response suppression control period and duty cycle preference.

A Inputs from LN5_M and AN1_M (orange and green shaded area) to LN3_M and output of LN3_M (red line) for 3 input delays from LN5_M to LN3_M (“rebound delay”, “ Δ ” in network schematic). The rebound delay is defined as the delay added to the output of LN5_M in the model. The effective delay between the AN1_M and LN5_M inputs to LN3_M depends on the pulse pattern (black, top, pulse duration 20ms, pause 18ms). An intermediate delay of 11ms produces the most overlap between the AN1_M and LN5_M inputs for that stimulus and hence the strongest responses in LN3_M. Vertical black line marks an AN1_M response peak, arrows point from the nearest LN5_M response peak.

B Preferred periods for LN3_M (red), LN4_M in an intact model (purple), and LN4_M in a model without inhibition from LN2_M to LN4_M (blue) as a function of the rebound delay. The preferred period increases with rebound delay for all three cases.

C Response fields for LN3_M (left), LN4_M in an intact network (middle), and for LN4_M in a model without inhibition in LN4_M from LN2_M (right) (color coded, see color bar). The rebound delay was set to 21 ms, which increases the preferred period in both LN3_M and LN4_M to 50 ms (left, compare B). However, increasing the delay also decreases the preferred duty cycle in LN4_M (middle). Removing the inhibition from LN2_M in LN4_M, abolishes the change in duty cycle preference (right). Anti-diagonal lines mark the preferred period of 50 ms for each response field and lines starting at the origin mark the preferred duty cycle.

D Same as B but for the preferred duty cycle. With increasing delay, the preferred duty cycle for LN4_M approaches 0.25 but is stable for LN3_M and for LN4_M without inhibition (see Fig. S3D).

E Inputs to LN4_M (middle, green: inhibition from LN2_M, red: excitation from LN3_M) and output of LN4_M (bottom, purple) for the intact network in C and for 3 different stimuli with a pulse period of 54ms and increasing duty cycles (top, black). Excitatory input from LN3_M is weaker and overlaps more with the inhibition for high duty cycles (compare amplitude and latency of response peaks in LN3_M), leading to a reduction in LN4_M responses with increasing duty cycle. Y-scales are identical for all three panels and were omitted for clarity.

F Dependence of peak amplitude (top) and peak latency (time from pulse onset to response peak, middle) of inputs to LN4_M (red: excitation from LN3_M, green: inhibition from LN2_M) on pulse duty cycle for the intact network in C. Weaker and later excitation suppresses LN4_M responses for pulse trains with high duty cycles (bottom, purple).

G Three sources of suppression in the network: The inhibitory lobe in the filter of AN1_M (green), adaptation in LN3_M (red), and inhibition in LN4_M from LN2_M (purple). Shown are responses of the respective neurons to a pulse pattern (top black, 20 ms pulse duration and 20 ms pause) when the source of suppression is present (dashed lines) or absent (solid lines). Removing suppression produces stronger or more sustained responses.

H Response fields (color coded, see color bar) for the network output (LN4_M) after removing different sources of suppression. The presence and absence of different sources of suppression is marked with a ‘+’ and a ‘-’,

respectively. Removing suppression in the network increases the preferred duty cycle. Lines mark the preferred pulse duty cycle and black circles indicate the preferred pulse duration and pause.

I Preferred duty cycles for models with different sources of suppression present (+) or absent (-) (see G).

The pulse trains for all simulations in this figure had a duration of 600 ms and were interleaved by chirp pauses of 200ms to ensure that trains contained enough pulses even for long pulse durations and pauses. Rebound delay set to 21ms in C and E-I to make changes in the duty cycle preference more apparent.

These results demonstrate that response suppression by inhibition in LN4_M becomes more effective at high duty cycles – longer pauses and shorter pauses – and is one source of the network’s bias towards low duty cycle preferences (Fig. 4C). We reasoned that other sources of response suppression, like inhibition or response adaptation elsewhere in the network, could further contribute to this bias.

Mechanisms of response suppression control duty cycle preference.

Three additional computational steps in the network could contribute to the bias against high duty cycles (Fig. 5G): First, the broad negative lobe of the filter in AN1_M (Fig. 2A, S1, S2) reduces responses to subsequent pulses in a train (Fig. 5G, green, S1A, B) because its effect accumulates over multiple pulses. Importantly, this suppression grows with the integral of the stimulus over the duration of the filter lobe and hence with the pulse duration and duty cycle. In AN1_M, this leads to shorter pulse responses due to thresholding and saturation by the output nonlinearity (Fig. S1D, S2). Second, the adaptation in LN3_M accumulates during and across pulses and reduces the neuron’s responses (Fig. 5G, red). This effect is again most prominent for pulse patterns with high duty cycles (long pulses, short pauses), since adaptation will be strongest during long pulses and recovery prevented during short pauses. Last, as discussed above, the inhibition from LN2_M also suppresses responses in LN4_M most strongly for stimuli with high duty cycle (Fig. 5G, purple).

To examine how the different sources of suppression shape the model’s tuning, we removed one or more of these computational steps: we set the negative lobe of the AN1_M filter to zero, we removed the adaptation from LN3_M, and we removed the inhibition forwarded from LN2_M to LN4_M (Fig. 5G). To accentuate the effects of these manipulations, we increased the delay of the LN5_M→LN3_M connection, which led to a preference for longer pulse periods (~50 ms) and for short duty cycles (~0.25) in LN4_M when all sources of suppression were present (Fig. 5H, left). Consistent with the prediction that different sources of suppression in the network reduce responses for stimuli with high duty cycles, the network’s preferred duty cycle tended to increase when suppression was removed (Fig. 5H, I). Removing one or two sources of suppression tended to induce more sustained responses during a pulse train (Fig. 5G) and to increase the preferred duty cycle from ~0.25 to ~0.50 (Fig. 5H, I). Removing all three sources of suppression abolished period tuning and produced a preference for constant tone stimuli with a duty cycle of 1.0 (Fig. 5H, right). Different sources of suppression sometimes interacted in unexpected ways. For instance, removing adaptation in AN1_M weakly decreased rather than increased duty cycle preference, because without adaptation, AN1_M produced stronger responses, which in turn induced stronger adaptation downstream in the network.

Overall, these results identify mechanisms of response suppression by adaptation and inhibition as a cause for the network preferring small duty cycles (short pulses and long pauses). They demonstrate how specific implementation details of a recognition mechanism constrain phenotypic diversity, but also reveal how different model parameters can be used to create phenotypic diversity by changing the preferred duty cycle (Fig. 5D, H, I). As a last step in our analysis, we examined a parameter that switches the preference type from period to duration tuning via changes in the rebound dynamics.

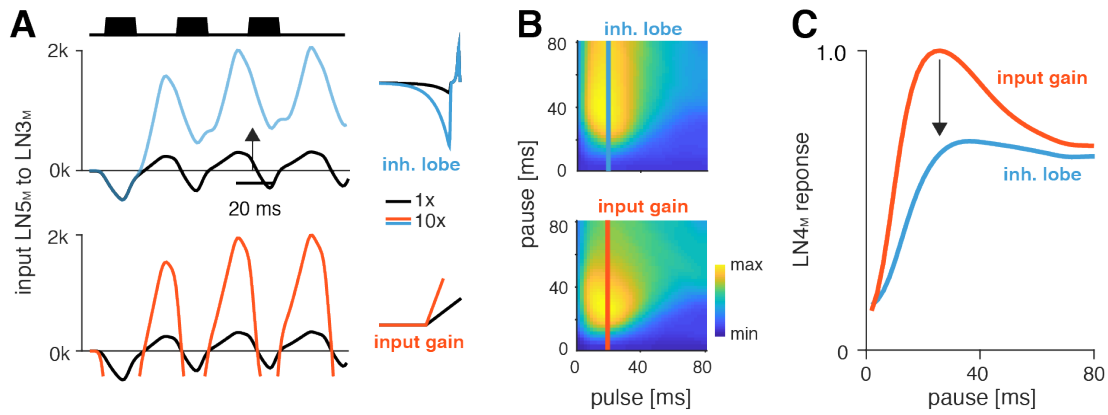


Figure 6: Changes in LN5_M rebound dynamics induce a switch in response type.

A Increasing the amplitude of the inhibitory lobe of the filter in LN5_M that generates the rebound (middle, blue, “inhibitory lobe”) increases the rebound’s amplitude and duration. By contrast, the gain of the input from LN5_M to LN3_M (bottom, red, “input gain”) amplifies the rebound without prolonging it. Pictograms on the right show the parameters for the original model (black) and for a model with a 10-fold increase in the respective parameter value (blue and red). Traces show the rebound inputs from LN5_M to LN3_M for the pulse pattern shown on top (black traces, 20 ms pulse duration and 20 ms pause). Negative response components are not part of the input to LN3_M but are plotted here for clarity.

B Response field of LN4_M for the models with increased inhibitory lobe (top) or input gain (bottom). Response magnitudes are color coded (see color bar, scaled to span the range of response magnitudes). Amplifying and prolonging the rebound by increasing the inhibitory lobe (top) produces pause tuning, while only amplifying the rebound via the input gain retains period tuning (bottom). Vertical lines correspond to the stimuli for which pause tuning curves are shown in C.

C Pause tuning curves for LN4_M at a pulse duration of 20 ms (see lines in B) reveal differential effects of the parameters on pause tuning. Amplifying and prolonging the rebound by increasing the inhibitory filter lobe (blue) produces high tolerance for pause duration, in this case high-pass tuning, which is required to obtain duration tuning. By contrast, only amplifying the rebound via the input gain (red) retains the preference for intermediate pauses characteristic for period tuning.

The pulse trains had a duration of 600 ms and were interleaved by chirp pauses of 200 ms for all simulations to ensure that the stimuli in the response fields contained enough pulses even for long pulse durations and pauses.

Changes in rebound dynamics can switch the preference type by engaging suppression.

Switches in preference type occur regularly even among closely related cricket species (Bailey et al., 2017; Hennig, 2003; Hennig et al., 2016), and we therefore looked for a model parameter that induced such a switch. We found that increasing the gain of the inhibitory lobe of the rebound filter in LN5_M (“inhibitory lobe” in short) (Fig. 6A, blue) switched the preference from period tuning to duration tuning (Fig. 6B, top), characterized by high tolerance for pause and high selectivity for duration (Fig. 1B). Increasing the inhibitory lobe parameter amplifies but also prolongs the rebound (Fig. 6A, blue) and we examined which of these two changes creates the switch from period to duration tuning. Other model parameters – like the gain of the input from LN2_M to LN5_M or from LN5_M to LN3_M (Fig. 6A, B, “input gain”, red) or the LN5_M output gain – only amplify the rebound and retain period tuning. This indicates that the amplification of the rebound is insufficient and that the prolongation of the rebound is necessary to cause the preference switch. In the original model, rebounds are short because the inhibition of LN5_M triggered by LN2_M activity always cuts off and suppresses rebound responses (Fig. 6A, black, see also Fig. 2E, F) and this happens even when the rebound is amplified (Fig. 6A, red). By contrast, in the model with an increased inhibitory lobe of the LN5_M rebound filter, the rebound persists during the LN2_M inhibition (Fig. 6A, blue). The prolonged rebound drives stronger adaptation downstream in LN3_M (Fig. S5), in particular for pulse patterns with short and intermediate pauses, because shorter pauses prevent recovery from adaptation in LN3_M. This response suppression for short and intermediate pauses abolishes the preference for intermediate pause durations necessary for period tuning and switches the preference type to duration tuning (Fig. 6C). This last analysis highlights the dual role of suppression in shaping the recognition phenotype of the network: Suppression constrains phenotypic diversity by reducing responses to patterns with long duty cycles (Fig. 4C, D, 5H, I) but it can also create phenotypic diversity by adjusting the network’s preferred duty cycle (Fig. 5H, I) or by switching the preference type (Fig. 6).

Discussion

How diversity in intraspecific communications systems is generated through the evolution of neural networks in the sender and in the receiver is an open question. Here, we asked whether the song recognition network revealed in *G. bimaculatus* (Schöneich et al., 2015) has the potential to generate the diversity of song recognition phenotypes known from crickets. In particular, we tested whether the delay-line and coincidence-detector network in *G. bimaculatus* can be considered a “mother network” for recognizing the song in different cricket species (Fig. 1) (Hennig et al., 2014). A model of the neuronal network reproduced the neuronal and behavioral data using simple, elementary computations like linear filtering, thresholding, saturation, and delays (Fig. 2, 3). Examining the model’s responses over a wide range of parameter values revealed that the network can generate all types of song preferences known from crickets and even other insects (Fig. 4A-E). We then identified key parameters that support and constrain the phenotypic diversity the network can produce, providing insight into how the network can be tuned to prefer different song parameters, such as pulse duration, pause, periods, or duty cycles (Fig. 4F-H, 5, 6).

The delay-line and coincidence-detector network can produce the full diversity of preference types in crickets.

Four principal preference types have been identified for song recognition in crickets and other insects (Fig. 1B): preference for pulse duration (Deutsch et al., 2019; Gray et al., 2016; Hennig, 2003), for pulse pause (Schul, 1998), for pulse period (Hennig, 2003; 2009; Rothbart and Hennig, 2012a; 2012b), and for duty cycle (Hennig et al., 2016). Variants of our network model produce all four of these preference types for the range of song parameter values relevant for crickets (Fig. 4A-E). This suggests that a delay-line and coincidence-detector network could form a common substrate – a “mother network” – for the diversity of song recognition phenotypes in crickets. Future studies will show whether the network can explain more complex preference functions known from crickets and other insects. For instance, preference types that betray resonant cellular or network properties are known from katydids (Bush and Schul, 2006; Webb et al., 2007) but it remains to be seen whether similar preference types exist in crickets. Several species of crickets produce complex songs that are composed of multiple types of pulse trains and it is unclear whether the current network can reproduce the known behavioral preference for such complex songs (Bailey et al., 2017; Cros and Hedwig, 2014; Hennig and Weber, 1997). In addition, we have not yet explored the network’s ability to reproduce the behavioral selectivity for parameters on the longer timescale of chirps or trills (Fig. 1A) (Blankers et al., 2016; Hennig et al., 2016).

How to tune a cricket song detector?

Our sensitivity analysis of the model identified three classes of parameters that define the model’s tuning (Fig. 4H). First, parameters that control the relative timing of inputs to the coincidence detector LN3_M set the network’s preferred pulse period. These include input delays in all upstream neurons (Fig. 5A, B) but also passive and active membrane properties that delay the rebound responses in LN5_M (Fig. S4). Second, parameters that lead to a stronger and more sustained rebound in LN5_M can shift the preference from pulse period to pulse duration tuning (Fig. 6). Lastly, sources of response suppression, like inhibition or adaptation, reduce responses to long pulses and high duty cycles (Fig. 5G-I). These three

classes of parameters account for changes within and transitions across the principal types of song preference in crickets. The model thus provides testable hypotheses for how response properties in the neuronal network may have evolved to compute the preference functions of different species. For instance, species that prefer either shorter or longer pulse periods than *G. bimaculatus* like *Teleogryllus leo* (Rothbart and Hennig, 2012a), *G. locorojo* (Rothbart and Hennig, 2012b), *G. firmus* (Gray et al., 2016), or *T. oceanicus* (Hennig, 2003) could differ in the delays of inputs to LN3 (Fig. 5B). Duty-cycle tuned species like *G. lineaticeps* or *G15* (Hennig et al., 2016) may exhibit weaker suppression throughout the network, for instance reduced adaptation in LN3 (Fig. 5G-I). Lastly, species with duration tuning such as *T. commodus* (Hennig, 2003) or *G13* (Gray et al., 2016) could exhibit longer and stronger rebound responses in LN5 (Fig. 6).

The three computations that define model tuning – response suppression, post-inhibitory rebounds, and coincidence detection – occur across species and modalities. Delay lines are prominent in binaural spatial processing (Schnupp and Carr, 2009) but have also been implicated in visual motion detection (Borst and Helmstaedter, 2015) or pulse duration selectivity in vertebrate auditory systems (Aubie et al., 2012; Buonomano, 2000). Suppression is known to act as a high-pass filter for pulse repetition rates (Baker and Carlson, 2014; Benda and Herz, 2003; Fortune and Rose, 2001) that in our case biases the network towards responding to rapidly changing patterns, like those with short pulses (Fig. 4C). Finally post-inhibitory rebounds have been implicated in temporal processing in different species like honeybees (Ai et al., 2018), fish (Large and Crawford, 2002), or mammals (Felix et al., 2011; Kopp-Scheinflug et al., 2018). The computations found to control the song preference in *G. bimaculatus* could therefore also govern pattern recognition in other acoustically communicating species.

We here only focused on modifications based on the magnitude of parameters, corresponding for instance to the expression levels of neurotransmitters or ion channels. Neuronal networks however, can also evolve to produce novel phenotypes by changing their topology, through a recruitment of novel neurons, a gain or loss of synapses, or switches in synapse valence from excitatory to inhibitory as has been shown in motor networks in *C. elegans* (Hong et al., 2019) and snails (Katz, 2011). In addition, we have not considered neuromodulators, which can rapidly alter network tuning (Bargmann, 2012; Marder, 2012; Marder et al., 2014), and which play a functional role in the phonotactic response (Poulet and Hedwig, 2005).

Implementation details reveal specific constraints

Previous studies revealed that Gabor filters can produce the full diversity of song preference functions found in insects (Clemens and Hennig, 2013; Clemens and Ronacher, 2013; Hennig et al., 2014). However, the computation giving rise to Gabor filters can be implemented with multiple mechanisms, each subject to specific constraints. For instance, the period tuning found in *G. bimaculatus* can be produced by the now known delay-line and coincidence-detection mechanism (Schöneich et al., 2015), but also by the interplay between precisely timed excitation and inhibition (Aubie et al., 2012; Rau et al., 2015), by cell-intrinsic properties like resonant conductances (Azevedo and Wilson, 2017; Rau et al., 2015), or by a combination of synaptic depression and facilitation (Fortune and Rose, 2001). By considering

the implementation of the pattern recognition algorithm in a particular species, we revealed a bias in the diversity of phenotypes that this specific implementation can produce: Several sources of suppression induce a bias towards preference for low duty cycle stimuli (Fig. 4B-D, 5G-I). This highlights the importance of studying nervous system function and evolution beyond the computational level, at the level of algorithms and implementations (Marr, 1982).

Functional tradeoffs limit behavioral diversity

The low duty cycle bias present in the recognition mechanism of *G. bimaculatus* has several implications for the evolution of song preference in crickets and elsewhere: Perceptual biases that have evolved in contexts like food or predator detection, are known to shape sexual selection (Guilford and Dawkins, 1993; Hofstede et al., 2015; Phelps and Ryan, 1998; Ryan and Cummings, 2013). In the case of song recognition in crickets, suppression (adaptation, inhibition, onset accentuation, Fig. 5G) reduces neuronal responses to long-lasting tones and likely evolved to save metabolic energy (Niven, 2016) or to make song recognition more robust to changes in overall song intensity (Benda and Hennig, 2008; Hildebrandt et al., 2011; Schöneich et al., 2015). As a side effect, adaptation now biases the song recognition mechanism towards preferring pulse trains with low duty cycles (Fig. 5H-I), which is consistent with the apparent absence of pause tuning in crickets (Hennig et al., 2014). Interestingly, pause tuning is known from katydids (Schul, 1998), suggesting that their song recognition system is not subject to the low duty-cycle bias. Katydids may have avoided the low bias either by using a delay-line and coincidence-detection network like that found in *G. bimaculatus* but with weaker suppression (Fig. 5G-I) or by using a different network design, that is subject to different constraints (Bush and Schul, 2005). Thus, computations that increase energy efficiency and robustness can constrain the phenotypic diversity of a whole species group.

From evolutionary pattern to process

How can a diversity of neural networks evolve to recognize the diversity of species-specific communication signals? Our modelling study of the song recognition network in the cricket brain provides first evidence that the underlying neuronal network is computationally flexible: by adapting physiological parameters it can produce all preference types described in crickets (Fig. 4B-E). The computational flexibility of the recognition mechanism may explain the species richness as well as the speed of evolution in a particular taxon like crickets (Alexander, 1962; Blankers et al., 2015; Desutter-Grandcolas, 2003; Oh and Shaw, 2013; Otte, 1992). However, computational flexibility also needs evolvability – the ability to generate specific phenotypes during evolution (Blankers et al., 2015). The “mechanistic degeneracy” of computation in biological neural networks – the fact that specific network outputs can be obtained by tuning disparate parameters – is thought to be a prerequisite for evolvability ((Wagner, 2011), see also (Hasson et al., 2020; Leonardo, 2005)). The degeneracy concept has been demonstrated extensively for motor networks (Gutierrez et al., 2013; Prinz et al., 2004), and here we also found evidence of degeneracy in the cricket song recognition network. For instance, the preferred pulse period (Fig. 5A, B, S4) or the pulse duty cycle (Fig 5G-I) can be set by multiple parameters. Future studies will employ novel computational methods for characterizing the high-dimensional parameter space (Bittner et al., 2019; Gonçalves et al., 2019) of our model to reveal possible evolutionary paths through the network’s parameter space. Our computational analyses need to be refined and

complemented by further electrophysiological experiments in *G. bimaculatus*, but crucially also in other species, to reveal the precise biophysical mechanisms that tune the network and to ultimately link changes in gene expression, e.g. of specific ion channels, to changes in network tuning.

References

- Ai, H., Kumaraswamy, A., Kohashi, T., Ikeno, H., and Wachtler, T. (2018). Inhibitory Pathways for Processing the Temporal Structure of Sensory Signals in the Insect Brain. *Front. Psychol.* *9*, 10624.
- Alexander, R.D. (1962). Evolutionary change in cricket acoustical communication. *Evolution* *16*, 443–467.
- Aubie, B., Sayegh, R., and Faure, P.A. (2012). Duration Tuning across Vertebrates. *Journal of Neuroscience* *32*, 6373–6390.
- Auer, T.O., Khallaf, M.A., Silbering, A.F., Zappia, G., Ellis, K., a, R.A.X.L.-O.X., Arguello, J.R., Hansson, B.S., Jefferis, G.S.X.E., Caron, S.J.C., et al. (2020). Olfactory receptor and circuit evolution promote host specialization. *Nature* *15*, 1–32.
- Azevedo, A.W., and Wilson, R.I. (2017). Active Mechanisms of Vibration Encoding and Frequency Filtering in Central Mechanosensory Neurons. *Neuron* 1–25.
- Bailey, N.W., Moran, P.A., and Hennig, R.M. (2017). Divergent mechanisms of acoustic mate recognition between closely related field cricket species (*Teleogryllus* spp.). *Animal Behaviour* *130*, 17–25.
- Baker, C.A., and Carlson, B.A. (2014). Short-Term Depression, Temporal Summation, and Onset Inhibition Shape Interval Tuning in Midbrain Neurons. *J. Neurosci.* *34*, 14272–14287.
- Baker, C.A., Clemens, J., and Murthy, M. (2019). Acoustic Pattern Recognition and Courtship Songs: Insights from Insects. <https://doi.org/10.1146/annurev-neuro-080317-061839> *42*, annurev-neuro-080317-061839.
- Bargmann, C.I. (2012). Beyond the connectome: How neuromodulators shape neural circuits. *Bioessays* *34*, 458–465.
- Benda, J., and Hennig, M.R. (2008). Spike-frequency adaptation generates intensity invariance in a primary auditory interneuron. *Journal of Computational Neuroscience* *24*, 113–136.
- Benda, J., and Herz, A.V.M. (2003). A universal model for spike-frequency adaptation. *Neural Computation* *15*, 2523–2564.
- Bittner, S.R., Palmigiano, A., Piet, A.T., Duan, C.A., Brody, C.D., Miller, K.D., and Cunningham, J.P. (2019). Interrogating theoretical models of neural computation with deep inference. *bioRxiv* *1050*, 837567.
- Blankers, T., Lübke, A.K., and Hennig, R.M. (2015). Phenotypic variation and covariation indicate high evolvability of acoustic communication in crickets. *Journal of Evolutionary Biology* *28*, 1656–1669.
- Blankers, T., Berdan, E.L., Hennig, M., and Mayer, F. (2018). Physical linkage and mate preference generate linkage disequilibrium for behavioral isolation in two parapatric crickets. *bioRxiv* 468538.
- Blankers, T., Gray, D.A., and Hennig, R.M. (2016). Multivariate Phenotypic Evolution: Divergent Acoustic Signals and Sexual Selection in *Gryllus* Field Crickets. *Evol Biol* 1–13.
- Borst, A., and Helmstaedter, M. (2015). Common circuit design in fly and mammalian motion vision. *Nature Neuroscience* *18*, 1067–1076.
- Bradbury, J.W., and Vehrencamp, S.L. (2011). *Principles of Animal Communication* (Sinauer Associates Incorporated).
- Buonomano, D.V. (2000). Decoding temporal information: A model based on short-term synaptic plasticity. *Journal of Neuroscience* *20*, 1129–1141.
- Bush, S.L., and Schul, J. (2006). Pulse-rate recognition in an insect: evidence of a role for oscillatory neurons. *Journal of Comparative Physiology a: Neuroethology, Sensory, Neural, and Behavioral Physiology* 1–9.
- Carlson, B.A., and Gallant, J.R. (2013). From Sequence to Spike to Spark: Evo-devo-neuroethology of Electric Communication in Mormyrid Fishes. *J Neurogenet* *27*, 106–129.
- Clemens, J., and Hennig, R.M. (2013). Computational principles underlying the recognition of acoustic signals in insects. *Journal of Computational Neuroscience* *35*, 75–85.
- Clemens, J., and Ronacher, B. (2013). Feature extraction and integration underlying perceptual decision making during courtship behavior. *Journal of Neuroscience* *33*, 12136–12145.
- Coffey, K.R., Marx, R.G., and Neumaier, J.F. (2019). DeepSqueak: a deep learning-based system for detection and analysis of ultrasonic vocalizations. *Neuropsychopharmacology* *231*, 1–10.
- Comins, J.A., and Gentner, T.Q. (2014). Temporal pattern processing in songbirds. *Current Opinion in Neurobiology* *28*, 179–187.

- Creutzig, F., Benda, J., Wohlgemuth, S., Stumpner, A., Ronacher, B., and Herz, A.V.M. (2010). Timescale-Invariant Pattern Recognition by Feedforward Inhibition and Parallel Signal Processing. *Neural Computation* 22, 1493–1510.
- Cros, E., and Hedwig, B. (2014). Auditory pattern recognition and steering in the cricket *Teleogryllus oceanicus*. *Physiological Entomology*.
- Destexhe, A., and Marder, E. (2004). Plasticity in single neuron and circuit computations. *Nature* 431, 789–795.
- Deutsch, D., Clemens, J., Thiberge, S.Y., Guan, G., and Murthy, M. (2019). Shared Song Detector Neurons in *Drosophila* Male and Female Brains Drive Sex-Specific Behaviors. *Current Biology* 29, 3200–3215.e3205.
- Ding, Y., Berrocal, A., Morita, T., Longden, K.D., and Stern, D.L. (2016). Natural courtship song variation caused by an intronic retroelement in an ion channel gene. *Nature*.
- Ding, Y., Lillvis, J.L., Cande, J., Berman, G.J., Arthur, B.J., Long, X., Xu, M., Dickson, B.J., and Stern, D.L. (2019). Neural Evolution of Context-Dependent Fly Song. *Current Biology* 0.
- Felix, R.A., Fridberger, A., Leijon, S., Berrebi, A.S., and Magnusson, A.K. (2011). Sound rhythms are encoded by postinhibitory rebound spiking in the superior paraolivary nucleus. *Journal of Neuroscience* 31, 12566–12578.
- Fortune, E.S., and Rose, G.J. (2001). Short-term synaptic plasticity as a temporal filter. *Trends in Neurosciences* 24, 381–385.
- Gentner, T.Q. (2008). Temporal scales of auditory objects underlying birdsong vocal recognition. *The Journal of the Acoustical Society of America* 124, 1350–1359.
- Gerhardt, C.H., and Huber, F. (2002). *Acoustic Communication in Insects and Anurans* (University Of Chicago Press).
- Goaillard, J.M., Taylor, A.L., Schulz, D.J., and Marder, E. (2009). Functional consequences of animal-to-animal variation in circuit parameters. *Nature Neuroscience* 12, 1424–1430.
- Gonçalves, P.J., Lueckmann, J.-M., Deistler, M., Nonnenmacher, M., Öcal, K., Bassetto, G., Chintaluri, C., Podlaski, W.F., Haddad, S.A., Vogels, T.P., et al. (2019). Training deep neural density estimators to identify mechanistic models of neural dynamics. *bioRxiv* 117, 838383.
- Desutter-Grandcolas, L. (2003). Phylogeny and the evolution of acoustic communication in extant Ensifera (Insecta, Orthoptera). *Zoologica Scripta* 32, 525–561.
- Gray, D.A., Gabel, E., Blankers, T., and Hennig, R.M. (2016). Multivariate female preference tests reveal latent perceptual biases. *Proc. R. Soc. B* 283, 20161972.
- Grobe, B., Rothbart, M.M., Hanschke, A., and Hennig, R.M. (2012). Auditory processing at two time scales by the cricket *Gryllus bimaculatus*. *J. Exp. Biol.* 215, 1681–1690.
- Guilford, T., and Dawkins, M.S. (1993). Receiver psychology and the design of animal signals. *Trends in Neurosciences* 16, 430–436.
- Gutierrez, G.J., O'Leary, T., and Marder, E. (2013). Multiple Mechanisms Switch an Electrically Coupled, Synaptically Inhibited Neuron between Competing Rhythmic Oscillators. *Current Biology* 77, 845–858.
- Hasson, U., Nastase, S.A., and Goldstein, A. (2020). Direct Fit to Nature: An Evolutionary Perspective on Biological and Artificial Neural Networks. *Neuron* 105, 416–434.
- Hennig, M.R. (2003). Acoustic feature extraction by cross-correlation in crickets? *Journal of Comparative Physiology a: Neuroethology, Sensory, Neural, and Behavioral Physiology* 189, 589–598.
- Hennig, M.R. (2009). Walking in Fourier's space: algorithms for the computation of periodicities in song patterns by the cricket *Gryllus bimaculatus*. *Journal of Comparative Physiology a: Neuroethology, Sensory, Neural, and Behavioral Physiology* 195, 971–987.
- Hennig, R.M., and Weber, T. (1997). Filtering of temporal parameters of the calling song by cricket females of two closely related species: a behavioral analysis. *Journal of Comparative Physiology a: Sensory, Neural, and Behavioral Physiology* 180, 621–630.
- Hennig, R.M., Heller, K.-G., and Clemens, J. (2014). Time and timing in the acoustic recognition system of crickets. *Frontiers in Physiology* 5.
- Hennig, R.M., Blankers, T., and Gray, D.A. (2016). Divergence in male cricket song and female preference functions in three allopatric sister species. *Journal of Comparative Physiology a: Neuroethology, Sensory, Neural, and Behavioral Physiology* 202, 347–360.

- Hildebrandt, K.J., Benda, J., and Hennig, R.M. (2011). Multiple Arithmetic Operations in a Single Neuron: The Recruitment of Adaptation Processes in the Cricket Auditory Pathway Depends on Sensory Context. *Journal of Neuroscience* 31, 14142–14150.
- Hofstede, ter, H.M., Schöneich, S., Robillard, T., and Hedwig, B. (2015). Evolution of a Communication System by Sensory Exploitation of Startle Behavior. *Current Biology* 25, 3245–3252.
- Hong, R.L., Riebesell, M., Bumbarger, D.J., Cook, S.J., Carstensen, H.R., Sarpolaki, T., Cochella, L., Castrejon, J., Moreno, E., Sieriebriennikov, B., et al. (2019). Evolution of neuronal anatomy and circuitry in two highly divergent nematode species. *eLife* 8, 1246.
- Katz, P.S. (2011). Neural mechanisms underlying the evolvability of behaviour. *Philos. Trans. R. Soc. Lond., B, Biol. Sci.* 366, 2086–2099.
- Kocher, T.D. (2004). Adaptive evolution and explosive speciation: the cichlid fish model. *Nat Rev Genet* 5, 288–298.
- Kopp-Scheinflug, C., Sinclair, J.L., and Linden, J.F. (2018). When Sound Stops: Offset Responses in the Auditory System. *Trends in Neurosciences* 41, 712–728.
- Kostarakos, K., and Hedwig, B. (2012). Calling song recognition in female crickets: temporal tuning of identified brain neurons matches behavior. *The Journal of Neuroscience : the Official Journal of the Society for Neuroscience* 32, 9601–9612.
- Kostarakos, K., and Hedwig, B. (2014). Pattern recognition in field crickets: concepts and neural evidence. *Journal of Comparative Physiology a: Neuroethology, Sensory, Neural, and Behavioral Physiology* 1–13.
- Kostarakos, K., Hartbauer, M., and R omer, H. (2008). Matched filters, mate choice and the evolution of sexually selected traits. *PLoS ONE* 3, e3005+–.
- Large, E.W., and Crawford, J.D. (2002). Auditory Temporal Computation: Interval Selectivity Based on Post-Inhibitory Rebound. *Journal of Computational Neuroscience* 13, 125–142.
- Leonardo, A. (2005). Degenerate coding in neural systems. *Journal of Comparative Physiology a: Neuroethology, Sensory, Neural, and Behavioral Physiology* 191, 995–1010.
- Marder, E. (2012). Neuromodulation of Neuronal Circuits: Back to the Future. *Neuron* 76, 1–11.
- Marder, E., O’Leary, T., and Shruti, S. (2014). Neuromodulation of Circuits with Variable Parameters: Single Neurons and Small Circuits Reveal Principles of State-Dependent and Robust Neuromodulation. *Annu. Rev. Neurosci.* 37, 329–346.
- Marr, D. (1982). *Vision: A Computational Investigation into the Human Representation and Processing of Visual Information* (Henry Holt & Company).
- Mendelson, T.C., and Shaw, K.L. (2005). Sexual behaviour: Rapid speciation in an arthropod. *Nature* 433, 375–376.
- Neunuebel, J.P., Taylor, A.L., Ben J Arthur, and Egnor, S.R. (2015). Female mice ultrasonically interact with males during courtship displays. *eLife* 4, e06203.
- Niven, J.E. (2016). Neuronal energy consumption: biophysics, efficiency and evolution. *Current Opinion in Neurobiology* 41, 129–135.
- Oh, K.P., and Shaw, K.L. (2013). Multivariate sexual selection in a rapidly evolving speciation phenotype. *Proceedings of the Royal Society B: Biological Sciences* 280, 20130482.
- Otte, D. (1992). Evolution of cricket songs. 1, 25–49.
- Phelps, S.M., and Ryan, M.J. (1998). Neural networks predict response biases of female túngara frogs. *Proceedings of the Royal Society of London. Series B, Containing Papers of a Biological Character. Royal Society (Great Britain)* 265, 279–285.
- Poulet, J.F.A., and Hedwig, B. (2005). Auditory orientation in crickets: pattern recognition controls reactive steering. *Proceedings of the National Academy of Sciences of the United States of America* 102, 15665–15669.
- Prieto-Godino, L.L., Rytz, R., Cruchet, S., Bargeton, B., Abuin, L., Silbering, A.F., Ruta, V., Peraro, M.D., and Benton, R. (2017). Evolution of Acid-Sensing Olfactory Circuits in Drosophilids. *Neuron* 0, 661–676.e666.
- Prinz, A.A., Bucher, D., and Marder, E. (2004). Similar network activity from disparate circuit parameters. *Nature Neuroscience* 7, 1345–1352.
- Ramdia, P., and Benton, R. (2010). Evolving olfactory systems on the fly. *Trends in Genetics : TIG* 26, 307–316.

- Rau, F., Clemens, J., Naumov, V., Hennig, R.M., and Schreiber, S. (2015). Firing-rate resonances in the peripheral auditory system of the cricket, *Gryllus bimaculatus*. *Journal of Comparative Physiology a: Neuroethology, Sensory, Neural, and Behavioral Physiology* 1–16.
- Riabinina, O., Dai, M., Duke, T., and Albert, J.T. (2011). Active process mediates species-specific tuning of *Drosophila* ears. *Current Biology : CB* 21, 658–664.
- Rothbart, M.M., and Hennig, R.M. (2012a). Calling song signals and temporal preference functions in the cricket *Teleogryllus leo*. *J Comp Physiol A* 198, 817–825.
- Rothbart, M.M., and Hennig, R.M. (2012b). The Steppengrille (*Gryllus spec./assimilis*): Selective Filters and Signal Mismatch on Two Time Scales. *PLoS ONE* 7, e43975.
- Ryan, M.J., and Cummings, M.E. (2013). Perceptual Biases and Mate Choice. *Annu. Rev. Ecol. Evol. Syst.* 44, 437–459.
- Ryan, M.J., Phelps, S.M., and Rand, A.S. (2001). How evolutionary history shapes recognition mechanisms. *Trends Cogn. Sci. (Regul. Ed.)* 5, 143–148.
- Schnupp, J.W., and Carr, C.E. (2009). On hearing with more than one ear: lessons from evolution. *Nature Neuroscience* 12, 692–697.
- Schöneich, S., Kostarakos, K., and Hedwig, B. (2015). An auditory feature detection circuit for sound pattern recognition. *Science Advances* 1, e1500325–e1500325.
- Schul, J. (1998). Song recognition by temporal cues in a group of closely related bushcricket species (genus *Tettigonia*). *Journal of Comparative Physiology a: Sensory, Neural, and Behavioral Physiology* 183, 401–410.
- Schulz, D.J., Goillard, J.M., and Marder, E. (2007). Quantitative expression profiling of identified neurons reveals cell-specific constraints on highly variable levels of gene expression. *Proc Natl Acad Sci U S A* 104, 13187–13191.
- Seeholzer, L.F., Seppo, M., Stern, D.L., and Ruta, V. (2018). Evolution of a central neural circuit underlies *Drosophila* mate preferences. *Nature* 544, 1.
- Turner, T.L., Miller, P.M., and Cochrane, V.A. (2013). Combining genome-wide methods to investigate the genetic complexity of courtship song variation in *Drosophila melanogaster*. *Mol Biol Evol* 30, 2113–2120.
- Wagner, A. (2008). Robustness and evolvability: a paradox resolved. *Proc. R. Soc. B* 275, 91–100.
- Wagner, A. (2011). The molecular origins of evolutionary innovations. *Trends in Genetics* 27, 397–410.
- Webb, B., Wessnitzer, J., Bush, S.L., Schul, J., Buchli, J., and Ijspeert, A. (2007). Resonant neurons and bushcricket behaviour. *Journal of Comparative Physiology a: Neuroethology, Sensory, Neural, and Behavioral Physiology* 193, 285–288.
- Weissman, D.B., and Gray, D.A. (2019). Crickets of the genus *Gryllus* in the United States (Orthoptera: Gryllidae: Gryllinae). *Zootaxa* 4705, 1–277.
- Wytenbach, R.A., May, M.L., and Hoy, R. (1996). Categorical Perception of Sound Frequency by Crickets. *Science* 273, 1542–1544.
- Xu, M., and Shaw, K.L. (2019). The Genetics of Mating Song Evolution Underlying Rapid Speciation: Linking Quantitative Variation to Candidate Genes for Behavioral Isolation. *Genetics* 211, 1089–1104.
- Zhou, J., Benson, N.C., Kay, K., and Winawer, J. (2019). Predicting neuronal dynamics with a delayed gain control model. *PLoS Comput Biol* 15, e1007484.

Methods

Electrophysiological data

The data used for fitting the model come from intracellular recordings with sharp microelectrodes of LN2-5 and are published in (Kostarakos and Hedwig, 2012) and (Schöneich et al., 2015). They include (1) 12 stimuli with a pulse duty cycle of ~ 0.5 and periods ranging from 22 to 86 ms (Fig. 2B), (2) 10 stimuli with a pulse period of 36 ms and duty cycles ranging between 0.06 and 0.94 (Fig. 2C), and (3) 12 stimuli with a pulse duration of 16 ms and pauses varying between 6 and 90 ms (Fig. 2D). During the electrophysiology experiments, each pulse train was presented interleaved by a chirp pause of 206 ms.

Quantification of tuning in the recordings and the model responses

In the recordings, spikes were detected using custom routines that found peaks in the voltage traces robust to changes in baseline. The accuracy of spike detection was checked by visual inspection of the voltage traces. From the spike times, average firing rates were calculated by dividing the number of spikes produced during each chirp (pulse train and chirp pause) by the chirp period (Fig. 2B-D). For the non-spiking LN5, the response corresponds to the voltage of the rebound responses. Accordingly, voltage rates were obtained by first calculating a baseline voltage as the average voltage in the 25 ms preceding a given pulse train, and then integrating the super-threshold components of the voltage. This integral voltage was then divided by the chirp period to get a voltage rate. Note that the tuning curves for LN5 are not very accurate because the baseline voltage fluctuated considerably during recordings of LN5.

For the model, tuning curves and responses fields were calculated as for the recordings – by integrating the firing rate outputs of the spiking neurons in the model or the rebound voltage for the non-spiking LN5 and dividing the resulting values by the chirp period.

Model inputs and simulation

We built a rate-based, phenomenological model of the song recognition network in *Gryllus bimaculatus*. Sound inputs were presented as the time-varying amplitude of pulse trains with the specified pulse and chirp structure. Model responses were simulated with a temporal resolution of 1kHz and tested as if pulse trains and chirp pauses were repeated endlessly.

Elementary computations

The model was built from four elementary computations, which are derived from neuronal processing. In the following, we will first define the elementary computations and then describe how they were combined to model each neuron in the network. Neurons in the model are referred to with a subscript “M”.

Filtering

Filtering was implemented via the convolution operation: $y(t) = \int_{-\infty}^t h(\tau)x(t-\tau)$, where $x(t)$ and $y(t)$ are the stimulus and response at time t , respectively, and τ is a temporal delay. The filter $h(\tau)$ was constructed from Gaussian and exponential functions. A Gaussian filter was defined as $h_g = \exp(-(\tau-N/2)^2/(4\sigma^2))$ with duration N , where $0 \leq \tau \leq N$, and width α such that $\sigma = (N - 1)/(2\alpha)$. Exponential filter functions were defined as $h_e = \exp(-\tau/\gamma)/\gamma$, with duration N , where

$0 \leq \tau \leq N$, and a time constant γ . Gaussian (Fig. S1A) and exponential filters are low-pass or integrating filters. They smooth the stimulus (Fig. S1B) and mainly differ in the temporal delay they add to responses – an exponential filter introduces no delays since it peaks at zero delay $\tau=0$, while a Gaussian filter induces a delay since it peaks at $\tau=N/2$. Band-pass filters were implemented as bi-phasic filters by either differentiating a Gaussian filter $\Delta(h(\tau)) = h(\tau) - h(\tau-1)$ (Fig. S1A) or by combining two Gaussian and/or exponential filters to form the positive and negative filter lobes. Differentiating filters respond most strongly to changes in the stimulus, for instance to the onsets or offsets of pulses (Fig. S1B). Note that most filters have a width or decay parameter (α or γ , respectively) and a duration parameter N . The width or decay parameters correspond to the standard deviation or decay constant of the Gaussian or exponential filters, respectively. The duration parameter is the duration over which the filter is defined and sets an upper bound on the width. If the duration is shorter than the width, then the resulting filter will be truncated. The duration parameter was initialized to be sufficiently long and was typically fixed during model fitting.

Nonlinearities

Nonlinearities transform inputs to implement thresholding or saturation. The model employs two types of nonlinearities: A rectifying nonlinearity thresholds the input x at the threshold value x_0 and scales it with a gain β : $y = \gamma\beta$ if $x > x_0$, $y=0$ otherwise (Fig. S1C). In many cases, the threshold parameter was used to constrain signals to be purely positive or negative and it was therefore often fixed to 0. A sigmoidal nonlinearity combines a soft threshold with saturation: $y = y_0 + y_{\max} / (1 + e^{-(ax - b)})$ with gain a , shift b and minimal and maximal output y_0 and y_{\max} , respectively (Fig. S1D).

Neuronal connections

Neuronal connections transmit neural activity linearly with delay Δ and gain β : $y(t) = \beta x(t-\Delta t)$. Multiple inputs to a neuron are added. The gain β is negative for inhibitory and positive for excitatory synapses and controls the input strength. The delay parameter Δ corresponds to the delay that needs to be added to the input of a neuron to reproduce the timing of the output of that neuron. It includes axonal conduction or synaptic transmission delays but also other delay mechanisms, like low-pass filtering of the membrane voltage at the pre- and post-synapse (Creutzig et al., 2010; Zhou et al., 2019) or latencies arising from integration of inputs to the spiking threshold or from spike generation.

Adaptation

Adaptation in AN1_M and LN2_M is implemented using differentiating filters (Fig. S1A, B). Such filters produce adaptation via their broad negative lobe, which suppresses subsequent responses. For LN3_M, adaptation effects were better captured using divisive normalization. The input to LN3_M is low-pass filtered using an exponential filter to generate an adaptation signal x_{ada} which divides the input: $y = x / (x_0 + w * x_{\text{ada}})$. x_0 and w control the strength of adaptation while the width of the exponential filter controls the timescale of adaptation.

Model neurons

The elementary computations described above were combined to reproduce the response of each neuron in the network – the firing rate patterns in the case of spiking neurons and the pattern of the rebound responses in the non-spiking LN5_M (Fig. 2E). All filters and

nonlinearities are plotted in Fig. 2A and all parameters names and values are listed in Table 1 and graphically defined in Fig. S1 and S2.

AN1_M (relay) and LN2_M (inhibition)

The input neurons of the network are AN1_M and LN2_M which faithfully copy the pulse structure and adapt weakly (Fig. 2E). These response properties were reproduced using a differentiating linear filter (Fig. S1): The filter's narrow and strong positive lobe captures the fast and faithful stimulus responses, while the broad negative lobe captures the delayed suppressive effect of past stimulus epochs. AN1_M's filter was generated by concatenating two Gaussians as the excitatory and inhibitory lobes. In LN2_M, an exponential function was used as the inhibitory lobe instead. AN1_M has a sigmoidal nonlinearity which saturates response to longer pulses. LN2_M has a rectifying nonlinearity which restricts outputs to be positives. For simplicity and since AN1 and LN2 produce similar responses, we used the output of LN2_M in lieu of AN1_M responses for all neurons postsynaptic to AN1_M.

LN5_M (post-inhibitory rebound)

LN5 is a non-spiking neuron. It receives inhibitory input coupled to the spike activity of LN2 and generates a rebound depolarization when the inhibition terminates (Fig. 2E). The inhibitory input from LN2 over a pulse saturates in LN5, which is modelled using a differentiating input filter followed by a rectifying nonlinearity that restricts the inputs to be negative. The rebound is then produced using a differentiating filter with a narrow positive lobe, which further low-pass filters the inhibitory input, and a broad negative lobe, which generates the broad positive voltage deflections at the offset of negative voltage deviations. See Fig. S1E for an illustration of the principle by which the rebound is produced in the model. The filter was generated by concatenating two exponential filters as inhibitory and excitatory lobes.

LN3 (coincidence detection)

LN3 responds strongly when two excitatory synaptic inputs arrive at the same time: a short-latency input from AN1 and a delayed input from LN5. For simplicity in the model we use the output from LN2_M, which largely copies the activity of AN1_M. In the neurophysiological data, the input from AN1 alone is often sufficient to drive spiking (e.g. to the first pulse of a train), suggesting that LN3 does not require two coincident inputs to spike. We therefore define LN3_M as a linear adder (with a threshold) that receives stronger input from AN1_M than from LN5_M. From LN5_M only the rebound was taken as the input to LN3_M, which was separated from the negative components of the LN5_M responses using a rectifying nonlinearity (Fig. S1C). The sum of the two inputs is thresholded using a rectifying nonlinearity before being passed into the adaptation stage with divisive normalization. The adaptation after summation reduces LN3_M firing over a pulse train, and a final rectifying nonlinearity ensures positive firing rates, by cutting off all negative responses that can occur in the model, for instance due to filtering (Fig. S1B).

LN4 (feature detection)

Finally, LN4_M linearly combines excitatory input from LN3_M and inhibitory input from LN2_M, which sharpens its tuning for pulse patterns as compared to LN3_M. A rectifying nonlinearity restricts the output firing rate to be positive.

Model fitting

Model parameters were optimized in two phases. First, the model parameters and structure were initialized by hand. This initialization established which computational steps were necessary to reproduce the key response features of the neurons in the network – their response dynamics and tuning – and determined initial parameter values.

In the second phase, we used a Genetic Algorithm to tune the network parameters to optimally fit the data, see Clemens et al., (2014). To simplify fitting, we exploited the feedforward topology of the network: Instead of fitting all parameters simultaneously, we adopted a stepwise procedure, in which the model neurons were fitted in order of their position in the network. We started with fitting the parameters of the first two neurons in the network (AN1_M and LN2_M) to reproduce the firing rate traces of LN2_M. The responses of AN1_M itself were not directly fitted since we did not have electrophysiological data for this thoracic neuron. However, we ensured that the responses of AN1_M – which are fairly similar to those of LN2 – were consistent with the literature (Kostarakos and Hedwig, 2012; Wohlers and Huber, 1982). In the second step, we held the parameters of AN1_M and LN2_M constant and fitted parameters of LN5_M. We fitted the temporal dynamics of the rebound response but not the inhibitory component, since the precise magnitude and dynamics of inhibitory components were highly variable across recordings and since the rebound constitutes the effective output of LN5. We then fitted the parameters of LN3_M and finally of LN4_M, again holding those of the upstream neurons constant. For these last two neurons, firing was very sparse and irregularly timed across trials, which complicated fitting. We therefore used information from the firing rate dynamics and from the tuning curves for optimizing the parameters of LN3_M and LN4_M, by using mixed error functions: $MSE_{traces} + w * MAE_{tuning}$ where MSE_{traces} is the mean square error between the predicted and actual traces, MAE_{tuning} is the mean absolute error between the predicted and the actual tuning curves, and w was set to 0.1 for LN3_M and to 1.0 for the even sparser activity of LN4_M. For the other neurons in the network (LN2_M, LN3_M, LN5_M), only MSE_{traces} was used (equivalent to $w=0$).

The initial parameters for fitting at each step were drawn from an exponential distribution ranging between 0.1 and 10 around the hand-fitted parameters. The exponential distribution was chosen to have an even number of parameters above and below the hand-fitted values, i.e. a uniform distribution after log scaling. While the fitting algorithm is stochastic by nature, it repeatedly found similar optimal parameter sets on independent initializations (not shown).

The model had a total of 51 parameters. Of these, 17 parameters (marked by “*” in Table 1) were fixed to the initialized values during fitting to facilitate convergence. For instance, a presynaptic neuron’s output and synaptic gain have identical effects on a given postsynaptic neuron and therefore only one of these parameters needs to be optimized. Or the duration parameter of an exponential filter sets an upper bound for the timescale of that filter, which in turn is given by the filter’s time constant. In that case, the duration was set to a sufficiently high value and fixed. Lastly, some of the thresholds were fixed to zero since their sole role was to fix firing rate outputs of the neurons to be positive.

Evaluation of model performance

After the fitting procedure, the model performance was evaluated based on the tuning curves and the response traces. The fit for the tuning curves was given by one minus the mean absolute error between the normalized tuning curves from the data and the model (Fig. 2H). Tuning curves of the data and the model were normalized to peak at 1.0. This performance measure does not take into differences in the overall scale of responses, and is 1.0 for a perfect match between the tuning curves and approaches 0.0 with increasing mismatch. The fit for the response traces was given by the squared correlation coefficient (r^2). The r^2 was calculated for different timescales (Fig. 2G) by low-pass filtering both the prediction and the response with rectangular windows with durations ranging between 1 ms and 25 ms before computing the r^2 . At short timescales, this measure is sensitive to fine details in the firing rate dynamics arising from precise spike timing, while at longer timescales, the measure reflects the match in coarser features of the firing dynamics, e.g. the spike counts per pulse.

Generation of model variants for the analysis of the parameter space

To determine the range of preference types the network can produce (Fig. 4A-E), we generated models with random parameter sets taken from a range around that obtained from the fit to *Gryllus bimaculatus*. For that, we chose 41 of the 51 model parameters. The ten parameters fixed for this analysis (marked by “+” in Table 1) had also been fixed for fitting (see above), but we allowed more of the parameters of AN1’s filter and output nonlinearity to change. All 41 parameters except the synaptic delay parameters were taken from a hypercube spanning the range between 1/10 and 10-fold around the original parameter set, spaced logarithmically such that the fraction of random parameter values below and above the original value was similar. Delay parameters in the model (see Table 1) were allowed to range uniformly between 1 and 21 ms, irrespective of the original parameter value. These parameters correspond to the delay added to the inputs to a neuron required to produce the desired timing of the output of that neuron and include axonal conduction and synaptic transmission delays, delays induced by low-pass filtering at the pre- and postsynapse, and delays from the integration of inputs to the spiking threshold and from spike generation. To ensure uniform sampling from the 41-dimensional parameter space, we used a quasi-random sampling scheme based on the Sobol set. We used the *sobolset* function in Matlab with the following parameters: skip 1e3, leap 1e2, scramble ‘MatousekAffineOwen’. Using this approach, we generated 1.58 million different model variants. Of these 90% (1.42 million models) were responsive and selective, that is, they responded to at least one pulse train pattern and did not produce the same response for all patterns tested. Initial tests with extended parameter ranges yielded qualitatively similar results in terms of the phenotypic variability but produced >50% unresponsive or unselective models.

Sensitivity analysis

For the sensitivity analysis (Fig. 4F-H, S3C) we changed either single parameters or systematically varied pairs of parameters on a grid. We used the same set of 41 parameters as in the analysis of the parameter space above (see Table 1). Single parameter sweeps were generated as 21 logarithmically spaced values between 1/100 to 100-fold around the original value, except for delay parameters, which were generated as 21 values ranging between 1 and 41 ms. While these parameter ranges may appear rather large, in particular for the input delay parameters, they are chosen to facilitate the detection of key parameters

controlling the network's tuning. Their specific and meaningful effects on the model tuning were confirmed and further analyzed within the more restricted parameter range also chosen for the analysis of the network's phenotypic flexibility above.

For each model we calculated the response fields for pulse durations and pauses between 1 and 80 ms (2 ms spacing, 1600 stimuli per response field), with a pulse train duration of 600 ms and a chirp pause of 200 ms. To quantify the model's sensitivity to changes in each parameter, we first calculated the correlation distance ($1 - \text{Pearson's correlation coefficient}$) between the response fields from the original model and each modified model in the parameter sweep (Fig. 4F). By using the correlation coefficient, our sensitivity analysis is robust to trivial changes in the response field like scaling or the addition of a constant to all responses. The average correlation distance over a parameter sweep is then taken as a measure of how much changing a parameter affects the model output.

For some parameters, models produced constant output (e.g. all zeros) over most of the parameter sweep with only one or two step-like changes in the response fields, leading to artificially high sensitivity values. We found that we could reliably exclude such parameters by calculating the median difference in the correlation distance between consecutive parameter values over the parameter sweep and requiring this quantity to be larger than 0.005. This also excluded parameters whose change produced largely untuned models over the sweep. We ensured that none of our results crucially depended on these criteria. For instance, even without the above constraint, the parameters of LN5_M and LN3_M were still among the top-ranked.

For the sensitivity analysis over parameter pairs (Fig. S3C), value grids were generated using the same value ranges as for single parameters for each parameter in the pair, resulting in $21 \times 21 = 441$ model variants for each of the 210 unique, unordered parameter pairs.

Identification of preference types

Response fields were assigned to one of the four principal types in Fig. 1B based on two inclusion criteria: First, the angle of the main axis had to fall within $\pm 5^\circ$ of that of the prototypical angle (-45° for period, 0° for duration, 45° for duty cycle, 90° for pause). Second, the response field had to be sufficiently selective for the designated stimulus parameter and tolerant for the orthogonal stimulus parameter. For instance, a response field was determined to be pause tuned if the angle was $\sim 90 \pm 5^\circ$, and if it was selective for pause and tolerant for duration. We ensured the validity of these criteria through visual inspection of many response fields (see examples in Fig. 4E).

For the first inclusion criterion, the orientation angle was calculated by fitting a line to the "ridge" of the response field, the set of pause and duration values that elicited maximal responses. We first identified well responded stimuli as those with response values exceeding 50% of the maximal response value for that field. To make the fits more robust, we determined whether the set of well-responded stimuli extended more along the pause or the duration axis and selected pause and duration values for the fit as follows: If the response field was most extended along the pause axis, then we identified the preferred

duration at each pause value for which the response field was above the 50% threshold. For a response field extended more along the duration axis we identified the preferred pause at each duration value exceeding the 50% threshold. We then fitted a line to the resulting set of duration and pause values and took the inverse tangent of that line's slope as the orientation angle.

For the second inclusion criterion, selectivity and tolerance were calculated from tuning curves extracted from transects crossing the response field's preferred duration and pause and cutting along the duration, pause, period and duty cycle directions. A Q-value was defined as the fraction of tuning curve values > 0.75 of the tuning curve's maximum value. A response field was only assigned to one of the four types if it's Q-value was > 0.5 for the parameter defining that type's (high Q = high sensitivity) and < 0.5 for the parameter corresponding to the orthogonal direction in stimulus parameter space (low Q = high tolerance).

Cell	Component	Parameters
AN1 _M	Filter excitatory lobe	(Gaussian) width $\sigma=0.46\text{ms}$, duration= 10ms^* , input delay 7.8ms^*
	Filter inhibitory lobe	(Gaussian) width $\sigma=2.19\text{ms}$, gain $\gamma=0.1$, duration $N=184\text{ms}^*$
	Output nonlinearity	(sigmoidal) slope= 1.5^* , shift= 1.5^* , gain=5, baseline= -0.5^*
LN2 _M	AN1 _M input	delay= 2ms^{*+} , gain= 1.0^{*+}
	Filter excitatory lobe	(Gaussian) width $\sigma=0.61$, duration $N=14\text{ms}$, gain= 0.26
	Filter inhibitory lobe	(exponential) decay $\gamma=5.24\text{ms}$, duration $N=1000\text{ms}^{*+}$
	Output nonlinearity	(rectifying) threshold= 0^{*+} , gain= 1.16
LN5 _M	LN2 _M input	delay= 8.7ms , gain= -0.0067
	Postsynaptic filter	(differentiated Gaussian) duration $N=5.0\text{ms}$, width $\sigma=(N-1)/7^{*+}$, gain of the excitatory lobe 1.1
	Postsyn. nonlinearity	(rectifying) threshold= 0^{*+} , gain= 1^{*+}
	Rebound filter exc. lobe	(exponential) decay 3.3ms , duration $N=21\text{ms}^*$, gain= 915
	Rebound filter inh. lobe	(exponential) decay 30ms , duration $N=500\text{ms}^{*+}$, gain= 1718
	Output nonlinearity	(rectifying) threshold= 0^{*+} , gain= 0.53
LN3 _M	AN1 _M input	delay= 7ms , gain= 36
	LN5 _M input	delay= 2ms , gain= 22
	Postsyn. nonlinearity	(rectifying) threshold= 0.081 , gain= 0.0129
	Adaptation	timescale $\tau=49\text{ms}$, strength $w=0.24$, offset $x_0=1^{*+}$
	Output nonlinearity	(rectifying) threshold= 2.48 , gain= 211
LN4 _M	LN2 _M input	delay= 1ms , gain= -547
	LN3 _M input	delay= 6ms , gain= 9.6
	Output nonlinearity	(rectifying) threshold 11236 , gain= 0.0022

Table 1 – Model parameters.

See Fig. S1 and S2 for an illustration and methods for a definition of all parameters. “*” marks parameters that were fixed during training (Fig. 2). “+” marks parameters that were fixed during parameter and sensitivity analyses (Fig. 4-6).

References in methods

- Clemens, J., Krämer, S., and Ronacher, B. (2014). Asymmetrical integration of sensory information during mating decisions in grasshoppers. *Proc Natl Acad Sci USA* *111*, 16562–16567.
- Creutzig, F., Benda, J., Wohlgemuth, S., Stumpner, A., Ronacher, B., and Herz, A.V.M. (2010). Timescale-Invariant Pattern Recognition by Feedforward Inhibition and Parallel Signal Processing. *Neural Computation* *22*, 1493–1510.
- Kostarakos, K., and Hedwig, B. (2012). Calling song recognition in female crickets: temporal tuning of identified brain neurons matches behavior. *The Journal of Neuroscience*, *32*, 9601–9612.
- Schöneich, S., Kostarakos, K., and Hedwig, B. (2015). An auditory feature detection circuit for sound pattern recognition. *Science Advances* *1*, e1500325–e1500325.
- Wohlers, D.W., and Huber, F. (1982). Processing of sound signals by six types of neurons in the prothoracic ganglion of the cricket, *Gryllus campestris* L. *Journal of Comparative Physiology A*, *146*, 161–173.
- Zhou, J., Benson, N.C., Kay, K., and Winawer, J. (2019). Predicting neuronal dynamics with a delayed gain control model. *PLoS Comput Biol* *15*, e1007484.

Supplemental figures

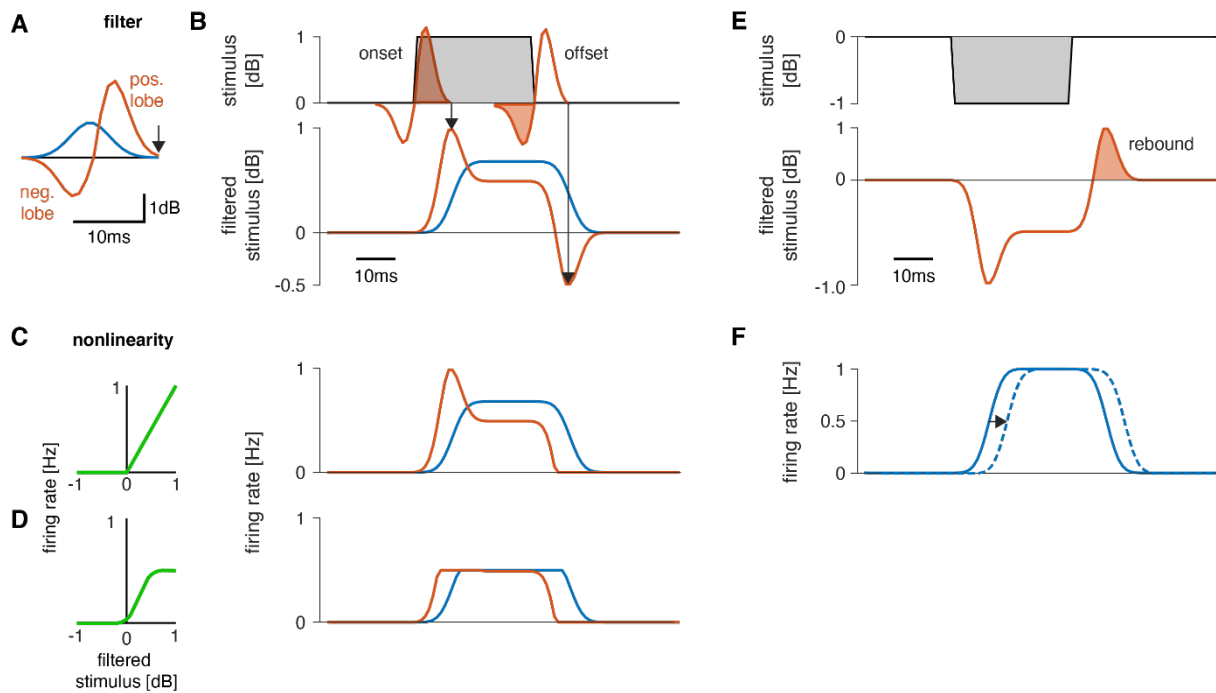


Figure S1: Working principle of filters and nonlinearities used as building blocks in the model.

A Shapes of a lowpass or integrating filter (blue) and of a bandpass or differentiating filter (orange). The integrating filter was generated from a Gaussian and the differentiating filter was obtained by taking the derivative of the integrating filter and scaling the negative filter lobe by $\frac{1}{2}$. A neuron's filter depicts the optimal stimulus pattern for strongly driving that neuron. The output is generated at the right end of the filter (arrow).

B Output of the two filters in A for a single pulse (top). The filtered stimulus (bottom) is generated by sliding the filter over the stimulus and computing the sum over the point-wise product between the filter shape and the stimulus. The filtered stimulus is produced at the right end of the filter (arrows). The integrating filter (blue) smooths the sharp on- and offsets of the pulse. The differentiating filter is a change detector because it responds strongly to changes in the stimulus (orange): A strong positive response occurs at pulse onset, because only the positive lobe is "activated" by the stimulus (indicated by the shaded part of the filter on top). A negative response at pulse offset arises because only the negative filter lobe overlaps with the pulse (shaded part of the filter on top). An intermediate response is produced during the pulse because the positive lobe is 2x larger than the negative lobe. A fully symmetrical filter would produce no response for constant stimuli irrespective of the stimulus amplitude. A differentiating filter produces phasic-tonic response pattern and is therefore useful for reproducing adapting responses in AN1_M, LN2_M, or for the inputs in LN5_M (see Fig. S2).

C A rectifying nonlinearity (left, green) with a threshold value of 0 cuts off all negative filter outputs.

D A sigmoidal nonlinearity (left, green) cuts off small and compresses large filter outputs. In the example, it compresses the onset accentuation and cuts off the negative offset response for the differentiating filter (orange). The responses for the differentiating (orange) and the integrating (blue) filter now mainly differ in their delay, with the differentiating filter leading the integrating filter, because the peak of the differentiating filter occurs closer to the time of the response (arrow in A).

E The response (bottom, dashed orange line) of the differentiating filter in A to a negative input (top) equals the sign-inverted response of that filter to a positive input (B). The positive response at pulse offset (shaded area) is used to reproduce the post-inhibitory rebound response of the LN5 neuron (see Fig. S2).

F Delayed transmission corresponds to the delay (arrow, solid lines: original input, dashed lines: delayed input) added to the inputs to a neuron required to reproduce the timing of the output of that neuron in the data.

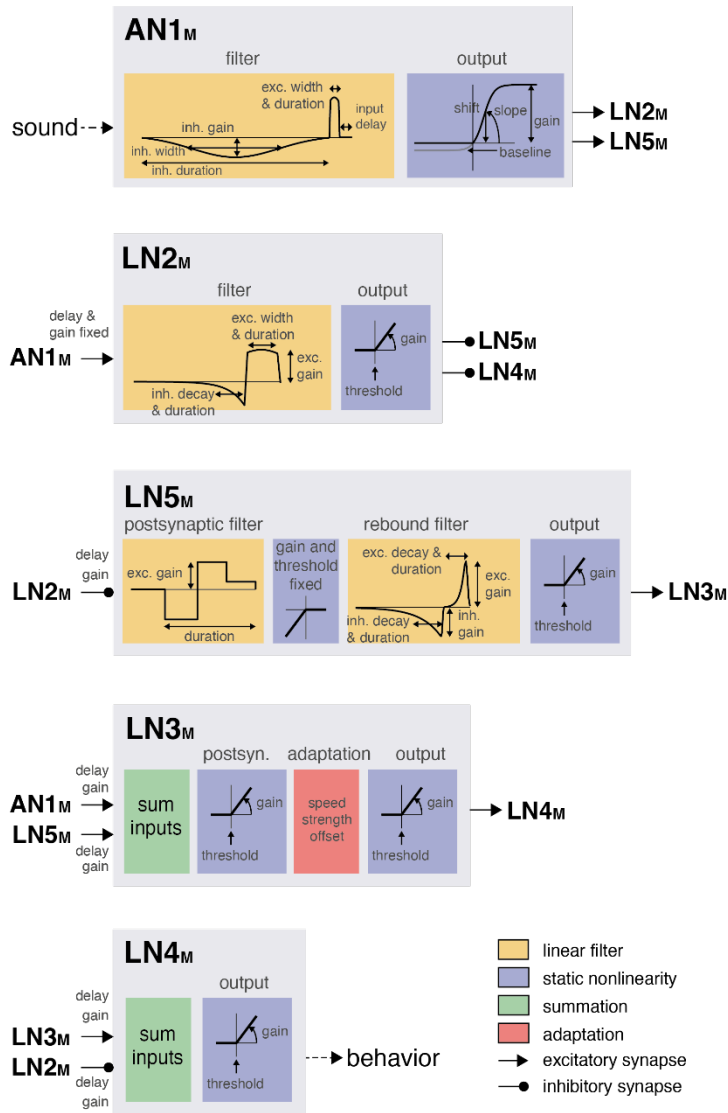


Figure S2: Illustration of the model parameters.

The model combines five elementary computations: linear filtering (yellow boxes), static nonlinearities (blue boxes), adaptation (red boxes), summation (green boxes), and delayed transmission (black lines, pointed arrowheads: excitatory inputs, round arrowheads: inhibitory inputs). The inhibitory lobe of the AN1_M filter is enlarged in the plot for clarity. See Table 1 in Methods for all parameter values and Fig. S1 for an illustration of the working principles of the filters, nonlinearities, and delayed transmission.

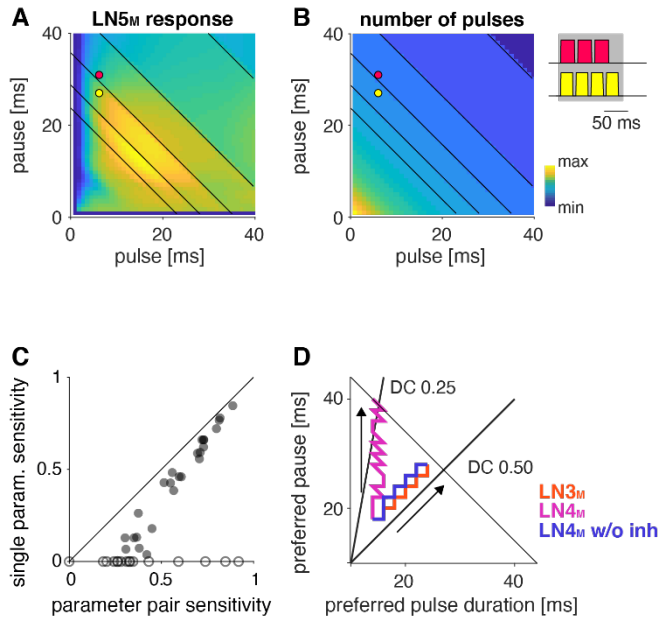


Figure S3: Origin of stepwise changes in the response fields, pair-wise sensitivity analysis, and impact of rebound delays in pulse-pause preference.

A, B Response field of LN5_M (A) and number of pulses per train in the underlying stimuli (B) (see color bar for color coding, color map was scaled to span the range of response values (A) and pulse numbers (B)). Changes in pulse number are marked by identical anti-diagonal black lines in both panels (only shown for pulse duration and pauses greater than 20 ms for clarity). Red and yellow dots in the fields in A and B refer to the two pulse train stimuli shown on the right of B with 3 pulses (red) and 4 pulses (yellow), and the maximal pulse-train duration of 140 ms is shown as a gray shaded area. Steps in the response fields (A, cf. Fig. 3) arise from stepwise changes in the number of pulses per train (B) due to the fixed pulse train duration.

C Sensitivity scores obtained from changing single parameters and parameter pairs are highly correlated ($r^2=0.95$) and top-ranked parameters are identical in the single and pair analyses. The sensitivity scores for single parameters were obtained by quantifying how much the response field of LN4_M changes when each of the 41 parameters selected for the analysis is changed individually (Fig. 4F). Sensitivity scores for pairs were obtained by changing pairs of parameters (see Methods). Open circles indicate parameters with zero sensitivity in the single parameter analysis and were excluded from the r^2 calculation.

D Preferred pulse and pause parameters for LN3_M (red), LN4_M (purple), and LN4_M without inhibition from LN2_M over the range of rebound delays tested in Fig. 5B, D (1-21 ms). Arrows point in the direction of increasing delays. The anti-diagonal line marks the pulse period of 50 ms and the diagonal lines mark the pulse duty cycles (DC) of 0.25 and 0.5. With increasing delay, the preferred duty cycle for LN4_M approaches 0.25 but is stable at around 0.45 for LN3_M and LN4_M without inhibition (compare Fig. 5D).

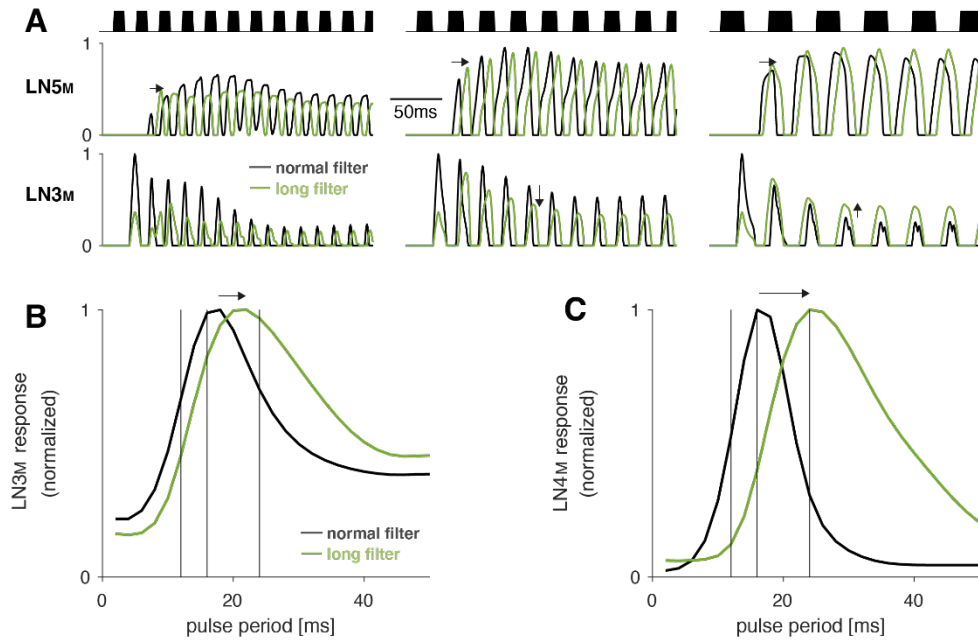


Figure S4: Increasing the duration of the postsynaptic filter in LN5_M delays rebound responses and increases the preferred pulse period in LN3_M.

A Rebound responses of LN5_M (top) and responses of the coincidence detector LN3_M (bottom) for models with a normal (black) and a long (green) postsynaptic filter in LN5_M (Fig. S2). The three stimuli (black) have pulse periods of 12, 16, and 24 ms and duty cycles of ~0.5. Increasing the filter duration delays rebound responses in LN5_M (middle row, arrows) and therefore shifts the pulse period at which LN3_M is most strongly driven towards higher values (bottom row, arrows).

B, C Period tuning of LN3_M (B) and of the network output LN4_M (C) for LN5_M with a normal (5ms, black) and a long (31ms, green) postsynaptic filter. The differentiating postsynaptic filter (Fig. S2) mediates adaptation and saturation of the inputs to the rebound filter in LN5_M (Fig. S1). Increasing the filter duration increases the preferred pulse period in LN3_M (B) and this effect is further amplified in LN4_M (C). Vertical black lines indicate the periods for the stimuli shown in A.

Response traces (A) and tuning curves (B, C) were normalized to peak at 1.0.

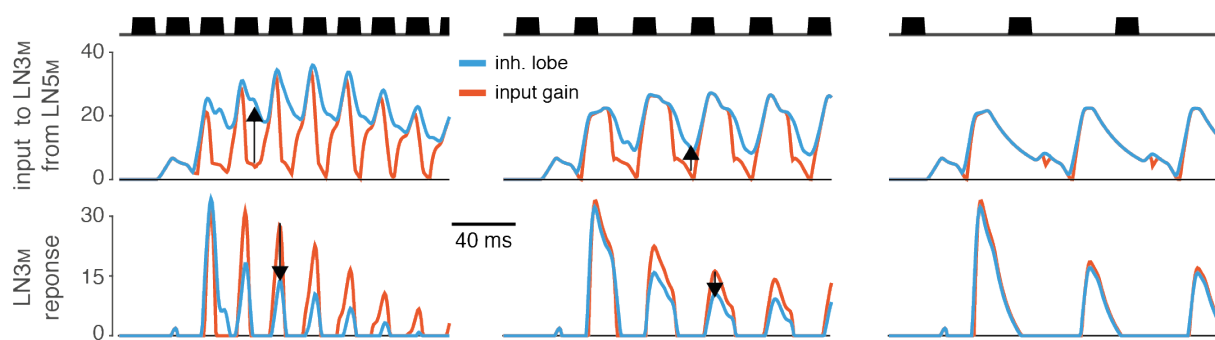


Figure S5: Sustained rebound responses in LN5_M induce stronger adaptation in LN3_M for short pauses. Traces of LN5_M→LN3_M inputs (middle) and LN3_M responses (bottom) for models with 10-fold increased input gain (red) or inhibitory lobe (blue). The sustained rebound response for pulse trains with short pauses in models with an increased inhibitory lobe (blue, middle) leads to stronger adaptation in LN3_M (blue, bottom). This reduces responses specifically for pulse patterns with short pauses (bottom, first two panels) and causes the switch from band-pass to high-pass tuning for pulse pause (Fig. 6). Arrows indicate changes of opposing sign in the input to LN3_M (middle) and the responses of LN3_M (bottom). Stimuli (top, black) have pulse durations of 10ms and pauses of 5, 15, and 35 ms.